Biomaterials Advances 134 (2022) 112688

Contents lists available at ScienceDirect

Biomaterials Advances

journal homepage: www.elsevier.com/locate/bioadv

PTH 1-34-functionalized bioactive glass improves peri-implant bone repair in orchiectomized rats: Microscale and ultrastructural evaluation

Pedro Henrique Silva Gomes-Ferreira [a,*], Chiara Micheletti [b], Paula Buzo Frigério [c], Fábio Roberto de Souza Batista [a], Naara Gabriela Monteiro [c], Odair Bim-júnior [d], Paulo Noronha Lisboa-Filho [d], Kathryn Grandfield [b,e], Roberta Okamoto [c,1]

[a] Department of Surgery and Integrated Clinic, São Paulo State University, Araçatuba Dental School, Araçatuba, SP, Brazil
[b] Department of Materials Science and Engineering, McMaster University, Hamilton, ON, Canada
[c] São Paulo State University, Araçatuba Dental School, Araçatuba, SP, Brazil
[d] Department of Physics, São Paulo State University, School of Sciences, Bauru, SP, Brazil
[e] School of Biomedical Engineering, McMaster University, Hamilton, ON, Canada

ARTICLE INFO

Keywords:
Osteoporosis
Bone regeneration
Parathyroid hormone
Dental implants
Bioactive glass
Local drug delivery

ABSTRACT

The objective of this work was to investigate the use of Biogran® functionalized with parathyroid hormone (PTH) 1–34 by sonochemistry for the local delivery of this anabolic agent to the implant site. The effects of Biogran® and topical administration of PTH 1–34 on peri-implant bone regeneration were evaluated from the microscale to ultrastructural levels in healthy (SHAM) and orchiectomized (ORQ). While some animals only received a titanium implant in their tibial metaphyses (CLOT group), in others the peri-implant defect was first filled with Biogran® either without or with PTH 1–34 functionalization (BG and BGPTH groups, respectively) prior to implant installation. Osseointegration was characterized from a biomechanical perspective by measuring the removal torque with the counter-torque technique. Micro-CT was used to evaluate the percentage of bone volume, trabecular thickness, number and separation, and bone-implant contact (BIC). Dynamics of new bone formation were assessed by measuring fluorochrome area, daily mineral apposition rate, and neoformed bone area using confocal laser microscopy. RT-PCR was performed to evaluate ALP and osteocalcin expression. The interface between newly formed bone and Biogran® was examined using scanning electron microscopy (SEM) and scanning transmission electron microscopy (STEM) at the micro-and nanoscale, respectively, while elemental analyses were completed in SEM with energy-dispersive X-ray spectroscopy (EDS). STEM imaging demonstrated the intimate attachment of bone to Biogran® (nanoscale level). Overall, the results suggest that the effectiveness of the topical administration of PTH 1–34 at the implant site seems enhanced in osteoporotic bone, promoting peri-implant bone regeneration to comparable levels in healthy conditions.

1. Introduction

Implant installation immediately after dental extraction is a common occurrence in deficient bone quality areas, such as dehiscences, fenestrations, and vertical and peri-implant defects, constituting a great part of the clinical conditions found in patients today [1]. In view of these situations, there is a need for improving bone reconstruction procedures to prepare or optimize the recipient bone through autogenous, xenogenous or alloplastic grafts [2].

Among alloplastic materials Biogran® (Biomet 3i, Palm Beach Gardens, Florida, USA) is a clinically available silica-based bioactive glass. Biogran® granules act as carriers for growth factors and serve as scaffold for bone formation [3,4]. Bioactive glasses have stood out as excellent osteoconductors, behaving superiorly to hydroxyapatite, as validated by the interaction between the biomaterial surface and adjacent bone tissue [5,6]. Biogran® has also been shown to be easy to manipulate and has displayed hemostatic properties, in addition to being more stable than hydroxyapatite in a bleeding site. Moreover, the silica content in bioactive glasses contributes further to their high bioactivity [7].

Not only the quantity, but also the quality of bone tissue is a determining factor for the proper integration of the dental implants [8–10]. In this context, when the bone exhibits a cortical and/or trabecular structure with lower density, the bone-implant interface is compromised [11,12], as it can be observed in osteoporosis [13,14]. Osteoporosis is a bone

* Corresponding author at: Rua José Bonifácio, 1193, 16015-050, Vila Mendonça, Aracatuba, Sao Paulo, Brazil.
E-mail address: pedroferreirabmf@gmail.com (P.H.S. Gomes-Ferreira).
[1] Roberta Okamoto is affiliated with research productivity scholarship (process: 306389/2017-7).

http://dx.doi.org/10.1016/j.msec.2022.112688
Received 15 August 2021; Received in revised form 20 January 2022; Accepted 27 January 2022
Available online 31 January 2022

metabolic disorder typically recognized as a significant health problem in women due to the depletion of estrogen supply in the post-menopausal phase, and affecting approximately 2/3 of this population [15,16]. However, osteoporosis is also regularly reported in men, with a higher incidence in individuals over 50 years of age [15–17].

Parathyroid hormone (PTH)-based medications are commonly indicated for severe osteoporosis, due to their anabolic properties able to increase bone mineral density [18]. In particular, PTH is an effective option for treating osteoporosis in men [18,19], and clinical studies have proved it to be successful at preventing vertebral and long bone fractures [20]. The use of topical PTH 1–34 has been tested in conjunction with titanium implants [20], showing that enough PTH was released locally from the implant surface to effectively influence the expression of osteoblastic genes, which suggests the potential efficacy of local delivery of PTH [21].

Metal ions used in scaffolds or processed in order to functionalize some surface showed osteoblastic and osteoclastic activity [22,23]. Zn-MS particles used in PLLA (Poly-L-lactic acid) scaffolds showed potential to improve mechanical properties and osteogenic activity [22]. Zinc silicate is also shown to be a promising additive to modify the osteogenic activity or even of other calcium phosphate ceramics (bone graft with low osteogenic activity and slow degradation rate) *via* macrophage immunomodulation [23].

Since the systemic use of PTH 1–34 is well described in the literature with positive outcomes on peri-implant bone regeneration and alveolar bone quality repair in rats [24,25]. In addition, previous work has shown that PTH 1–34 can be used to functionalize bioactive glass using sonochemistry [26]. This work aims to evaluate the effect of the local release of PTH 1–34 as functionalized to Biogran® by sonochemistry on peri-implant bone regeneration in osteoporotic conditions through analyses on calcified tissue, biomechanics, and the nanoscale ultrastructural evaluation of the bone-biomaterial interface formed in the reparation process.

2. Materials and methods

2.1. Animals

After approval by the Ethics Committee on the Use of Animals of the Araçatuba Dental School at UNESP (approval no. 00199/2017), 80 6-month-old male rats (Rattus novergicus albinus, Wistar) from the central vivarium of the Araçatuba Dental School at UNESP, weighing around 500 g, were used. The animals were randomly allocated in two groups (SHAM and ORQ), according to gonadectomy surgery. Rats assigned to the SHAM group were subjected to fictitious surgery, with exposure of the testicles only, while those in the ORQ group underwent bilateral orchiectomy.

Both ORQ and SHAM groups were further divided into three different subgroups: CLOT, receiving the implant only, without the use of Biogran®; BG, receiving Biogran® in the peri-implant defect, in addition to the implant; and BGPTH, receiving Biogran® functionalized with PTH 1–34, in addition to the implant (Table 1).

Prior to surgery, all the animals were kept in individual cages and fed a balanced diet (NUVILAB, Curitiba PR, Brazil) containing 1.4% Ca and 0.8% P, and water *ad libitum*.

2.2. Biomaterial, preparation and functionalization by sonochemistry

Biogran® (Biomet 3i, Palm Beach Gardens, Florida, USA) with a particle size of approximately 300 to 355 μm was used, this biomaterial is a silica-based bioactive glass, it has a osteoconductive characteristic, made of SiO_2(45 wt%), CaO (24.5 wt%), Na_2O (24.5 wt%) and P_2O_5 (6 wt%). The functionalization was performed using Biogran®, PTH 1–34 (Forteo®, Ely Lilly, Indianapolis, Indiana, USA), presented in liquid form in a concentration of 250 μg/ml in an injection pen with a cartridge of 3 ml, and Milli-Q® ultrapure water were mixed together by sonochemistry to obtain a homogeneous mixture and to decrease the particle size of the ceramic using the methodology described in thorough detail elsewhere [26]. Briefly, the above components were subjected to ultrasonic processing in a Sonics VCX-750 model, with 750 W of power and frequency of 20 kHz, with 3 pulses of 5 min (for a total 15 min of sonochemistry, which was previously shown to provide the best physiological response [25]) and variable amplitude fixed up to 40% of the nominal amplitude of the equipment (450 W/cm^2). In the synthesis chamber, the conditions were atmospheric air, whereas the container with the samples and the ultrasonic tip were cooled with an ice bath. For the BG group, a similar process was used but with Biogran® particles and Milli-Q® water only, without the addition of PTH 1–34. After sonochemistry the samples were subsequently dried in an oven at 60 °C, and no further thermal annealing treatment was carried out [26–28].

Table 1
Experimental groups according to the biomaterial experiment and test.

Groups	
CLOT	Group in which the peri-implant defect was created and an implant installed without the use of Biogran®.
BG	Group in which the peri-implant defect was created and an implant installed after filling the defect with Biogran®.
BGPTH	Group in which the peri-implant defect was created and implant installed after filling the defect with Biogran® functionalized with PTH 1–34.

After implantation of the biomaterial, a fraction of PHT molecules adsorbed on the outermost layers of glass particles will inevitably be released to the physiological environment. Another fraction of the drug will probably undergo sustained release as the bioactive glass dissolves *in situ*. It is known that when a surface-active silicate glass is immersed in body fluids, a sequence of inorganic stages leads to the partial dissolution of the glass, which is critical to the bone-bonding ability of these materials [29]. Furthermore, it is expected that the sonochemical treatment promotes an effective chemical bond between PTH (O) and the BG's surface (Si or P), as reported in the literature [30].

Otherwise, time-dependent release curves have also been reported with a drug release (in %) about of 50% after 30 h [31], in a similar behavior already reported by elsewhere [30].

2.3. Animal surgeries

2.3.1. Bilateral orchiectomy

After anesthesia with Coopazine (Xylazine-Coopers, Brasil, Ltd.) and Vetaset (injectable ketamine hydrochloride, Fort Dodge, Saúde Animal Ltd.), both scrotal sacs of the ORQ rats were incised to expose the testicles. Using hemostatic forceps, the spermatic funicular was presented, with concomitant individualization and ligation of the vas deferens and the vascular pedicle, and then sectioned. The testicles were removed and the surgical wound was sutured with polyglactin 910 4-0 (Ethicon, Johnson & Johnson, São José dos Campos, SP, Brazil). The SHAM group underwent the same procedure, but only the surgical exposure of the testicles was performed without their removal, in order to subject the animals in this group to the same surgical stress as the ORQ group [32]. The rats were kept in the Vivarium of the Basic Sciences Department of the Araçatuba Dental School at UNESP. This same surgical technique has already proved to be effective at inducing osteoporosis in other studies [24,25,33].

2.3.2. Peri-implant defect surgery and implant installation

Peri-implant defect surgery and implant installation occurred 30 days after orchiectomy and fictitious surgeries. The animals were fasted for 8 h prior to the surgical procedure and sedated by a combination of 50 mg/kg intramuscular ketamine (Vetaset, Fort Dodge Saúde Animal Ltd., Campinas, São Paulo, Brazil) and 5 mg/kg xylazine hydrochloride (Dopaser, Laboratorio Calier do Brasil Ltd., Osasco, São Paulo, Brazil), and they received mepivacaine hydrochloride (0.3 ml/kg, Scandicaíne 2% with adrenaline 1: 100,000, Septodont, France) as local anesthesia and for hemostasis of the operative field. After sedation, trichotomy was performed in the medial portion of the tibia and antisepsis was ensured with Polyvinyl Pyrrolidone Iodine (PVPI 10%, Riodeine Degermante, Rioquímica, São José do Rio Preto). A 1.5 cm long incision was made in

the region of the tibial metaphysis bilaterally with a blade number 15 (Feather Industries Ltda, Tokyo, Japan) and the bone was exposed.

Commercially pure grade IV titanium implants (Emfils Comércio Produtos Odontológicos) (Ø = 2 mm, L = 4 mm) with a surface treated by double acid etching were installed in the tibia after sterilization by gamma irradiation. A defect was created using the technique by Gomes-Ferreira et al. [26], *i.e.*, with a 1.3 mm diameter cutter on the two cortices, and a 2.0 mm, a pilot (2/3) and a 3.0 mm cutter on the upper cortex. In the CLOT group the implant was immediately inserted in the defect and locked in the lower cortex only. Conversely, implants in the BG and BGPTH groups were placed and locked into the lower cortex after the defect void was filled by Biogran® (with or without PTH functionalization). The volume of biomaterial used to fill the defect sites in the BG and BGPTH groups was computed from estimating the defect volume as a cylinder (L = 4 mm, radius = 3 mm cutter diameter/2, hence V = 28.27 mm^3), minus the volume of the implant estimated as a cylinder (L = 4 mm, radius = 2 mm, hence V = 12.57 mm^3). Therefore, a total of 15.7 mm^3 of Biogran® was inserted in the defect, which ensured contact with the implant throughout its length.

The relative mass concentration of PTH 1–34 and Biogran® in the BGPTH group was determined as described in [34], where 1 μg of PTH 1–34 was used for every 35.34 mm^3 of Biogran®. Therefore, a 15.7 mm^3 defect as used herein contains 0.44 μg of PTH 1–34, or about 2 μl.

A total of 128 implants were placed across all groups. Each animal received two implants, one in each tibial metaphysis. The tissues were sutured in planes using absorbable thread (Polygalactin 910 - Vycril 4.0, Ethicon, Johnson Prod., São José dos Campos, Brazil) with continuous stitches in the deep plane and with monofilament thread (Nylon 5.0, Ethicon, Johnson, São José dos Campos, Brazil) with interrupted points in the outermost plane.

In the immediate postoperative period, each animal received a single intramuscular dose of 0.2 ml of penicillin G-benzathine (Small Veterinary Pentabiotic, Fort Dodge Saúde Animal Ltd., Campinas, SP). The animals were kept in individual cages throughout the experiment with food and water *ad libitum*.

2.3.3. Implant and retrieval timeline

On the 30th day after ORQ and SHAM surgeries, surgery for the creation of bone defect and installation of the implants in the tibiae of the rats was performed. For elemental and ultrastructural analyses, euthanasia was performed 30 days after implant placement. For biomechanical, reverse transcriptase-polymerase chain reaction (RT-PCR), micro-computed X-ray tomography (micro-CT), and confocal laser microscopy analyses, 14 days after implant installation 20 mg/kg of the fluorochrome calcein was administered intramuscularly [35,36], and after another 28 days (*i.e.*, 42 days after implant placement) 20 mg/kg of the fluorochrome alizarin red was administered to each animal [35,36]. These animals were then euthanized at 60 days after implant placement (18 days after alizarin administration).

2.4. Biomechanical analysis

For biomechanical analysis, 8 animals from each group (CLOT, BG, BGPTH groups for both ORQ and SHAM) had the metaphyses of the left tibias reopened to expose the implants and perform removal torque. An implant mount (Conexão, São Paulo, Brazil) was adapted to the implant hexagon and a digital torque wrench was coupled to the implant mount. Counterclockwise motion was applied, increasing the reverse torque until rotation of the implant inside the bone tissue occurred, completely breaking the bone-implant interface. When the torque wrench registered the maximum torque peak for this break, expressed in Newton centimeters (N.cm), this value was noted and tabulated for further statistical evaluation.

2.5. RT-PCR

After removal torque experiments, bone tissue from the tibial region previously in contact with the implant was extracted to assess the genes associated with bone maturation at 60 days using RT-PCR. The tissue was rinsed with phosphate buffered saline (PBS), frozen in liquid nitrogen and stored at −80 °C prior to ribonucleic acid (RNA) extraction. The SV Total RNA Isolation System kit (Promega, Madison, Wisconsin, USA) was used for RNA extraction, followed by quantification, concentration and purity analyses.

Normalization of the total RNA concentration was performed, followed by the manufacture of complementary strands of deoxyribonucleic acid (cDNA) (Sigma-Aldrich, St. Louis, Missouri, USA). The expression of genes related to bone repair, *i.e.*, alkaline phosphatase (ALP) and osteocalcin (OC), was assessed by RT-PCR using the SybrGreen System method (Applied Biosystems, Foster City, California, USA). Taqman Universal PCR Master Mix was added to the plates containing the genes of interest. The reactions were repeated in quadruplicates and the cDNA volumes were calculated according to the quantification of the samples. The amplification reaction was performed, and the results analyzed based on the value of the cycle threshold (Ct), which allowed the quantitative analysis of the expression of genes of interest, as well as the related genes on the plate [24].

2.6. Micro-CT

Implants and surrounding bone from the right tibia (n = 8 per group) were retrieved and trimmed, fixed in a 10% buffered formalin solution (Analytical Reagents, Dinâmica Odonto-Hospitalar Ltd., Catanduva, SP, Brazil) for 48 h, rinsed under running water for 24 h, and then stored in 70% ethanol. Micro-CT was completed (SkyScan 1272 Bruker MicroCT, Aatselaar, Belgium) using 8 μm-thick cuts with a 90 kV X-ray beam, a 111 μA current, a 0.5 mm Al filter and a 0.4° rotation step. Images were recorded with a 2016 μm × 1344 μm resolution over 1 h and 38 min acquisition time. Data were reconstructed using the NRecon software (SkyScan, 2011; Version 1.6.6.0), applying a smoothing factor of 5, a correction of the artifact rings of 7, and a beam hardening correction equal to 40%. The Data Viewer software (SkyScan, Version 1.4.4 64-bit) was used to visualize the reconstructed volumes in the transversal, longitudinal and sagittal planes. The CT-Analyser (CTAn) software (SkyScan, 2012; Version 1.12.4.0) was used to determine the percentage of bone volume over total volume (BV/TV), the trabecular thickness (Tb.Th), trabecular separation (Tb.Sp) and trabecular number (Tb.N), in addition to the bone-implant contact (BIC) through the intersection surface (i.S) for 3D reconstruction by CTvox software (SkyScan, Version 2.7).

2.7. Preparation of calcified tissues

After micro-CT analysis, the samples were progressively dehydrated in ethanol (70%, 80%, 90% and 100%) changing the solution every 5 days in an orbital shaker every day for 4 h. At the end of dehydration, the pieces were immersed in a mixture of 100% alcohol and Techno Vit® light-curing resin (Kulzer GmbH, Hanau, Germany) in different concentrations, until only resin remained as an immersion medium, and the Technovit resin was light-cured. Embedded blocks were then cut along the medio-distal plane using a cutting system (Exakt Cutting System, Apparatebau, Gmbh, Hamburg, Germany) and polished using an established protocol until the cross-section was approximately 80 μm thick.

2.8. Confocal laser microscopy

Longitudinal cuts were obtained at the bone/implant interface region corresponding to the third, fourth and fifth turns of the implants. These sections were imaged by a Leica CTR 4000 CS SPE confocal laser microscope (Leica Microsystems, Heidelberg, Germany), using a 10× objective (original increase 100), to detect the fluorochromes calcein and alizarin red. The daily bone mineral apposition rate (MAR) and neoformed bone area (NBA) were calculated on the third thread on each side of the implant, following the method reported in [37].

The images were analyzed in ImageJ (National Institutes of Health, Bethesda, Maryland, USA) using the “freehand selection” tool to measure the area of the fluorochromes and the NBA. The “straight line” tool was

employed to complete 5 measurements from the outer margin of the calcein area towards the outer margin of the alizarin red area. The values obtained were then divided by 28 (time interval in days between the two injections of fluorochromes) in order to evaluate the MAR, as described in [38].

2.9. Elemental and ultrastructural analyses

The response of the biomaterial to the bone regeneration process in the peri-implant defect with or without functionalization with PTH 1–34 was evaluated within 30 days. For this purpose, 8 animals per group (ORQ - BG and BGPTH; and SHAM - BG and BGPTH) were submitted to the same surgeries previously mentioned, but with euthanasia time reduced to 30 days in order to assess the peak of bone neoformation before remodeling. These samples were embedded in Techno Vit® resin and cut in half by the EXAKT cutting system as described above before further preparation and ultrastructural analysis. It is important to note that the CLOT group, both SHAM and ORQ, was not included, since the objective of this analysis was to evaluate the bone-biomaterial interface with or without PTH 1–34 functionalization. The sample block was polished using 400 to 2400 grit silicon carbide paper to expose the cross section of the bone-biomaterial interface. The samples were fixed to SEM stubs with carbon tape, wrapped in aluminum tape, and then painted with nickel when necessary. Later, they were coated with a thin layer of carbon (~10 nm) to improve the conductivity in the SEM. The workflow of all electron microscopy characterizations at the bone-Biogran® interface is described in detail by Micheletti et al., [39] but the main steps are reported herein.

2.9.1. Scanning electron microscopy (SEM)

SEM imaging was completed by acquiring secondary (SE) and backscattered electron (BSE) images using a JEOL 6610LV (JEOL Ltd., Japan) and an FEI Magellan 400 XHR (ThermoFisher Scientific, Hillsboro, USA) SEMs operated at an acceleration voltage of 5 kV. Compositional contrast in BSE images allowed for the distinction between biomaterial and bone based on atomic number. The images were recorded in several enlargements around the implant for later selection of the best bone-biomaterial contact areas for the next stage of analyses.

2.9.2. Energy dispersive X-ray spectroscopy (EDS)

In the same sample, using an FEI Magellan 400 XHR SEM (ThermoFisher Scientific, Hillsboro, USA) the elemental analysis was determined by EDS operated at 10 kV. EDS data was collected using an 80 mm^2 X-Max detector (Oxford Instruments, Concord, MA, USA) and processed using AZtec software (Oxford Instruments, Concord, MA, USA). Elemental maps were obtained for Biogran® to search for compositional changes in Ca, P and Si and to generate line profiles for compositional changes across the biomaterial.

2.9.3. Focused ion beam (FIB) and scanning transmission electron microscopy (STEM)

After identifying regions of bone in contact with Biogran® particles with SEM, a dual beam focused ion beam (FIB) instrument (Zeiss NVision 40, Carl Zeiss AG, Oberkochen, Germany) was used to prepare electron transparent (100–200 nm thick) specimens for STEM analysis using an *in situ* lift-out protocol,[†] and shown step-by-step for the ORQ BG group in Fig. 1. The resultant average sample size extracted from the block was 10 μm × 6 μm, thus being large enough to analyze nano-osteoconduction.

STEM imaging was done in a Titan 80–300 instrument (ThermoFisher Scientific, Hillsboro, USA) operated at 300 kV with a high-angle annular dark field (HAADF) detector. In this form of image, the contrast is proportional to the atomic number, which allows us to record images without the use of heavy metal stains that alter bone chemistry.

2.10. Immunohistochemical analysis

Additional animals were used to perform the osteoclast evaluation through immunohistochemical analysis. The samples were reduced and fixed in 10% formaldehyde (Analytical Reagents, Dinâmica Odonto-Hospitalar Ltda, Catanduva, SP, Brazil) for 48 h, washed in running water for 24 h and demineralized in 10% EDTA. Then, the samples were dehydrated with a sequence of alcohols and diaphanized in xylol and then included in paraffin. Cuts with thickness of 5 μm were obtained.

The reaction was performed on four pieces (left tibias) per group, using the indirect immunoperoxidase method with an amplifier. To inhibit

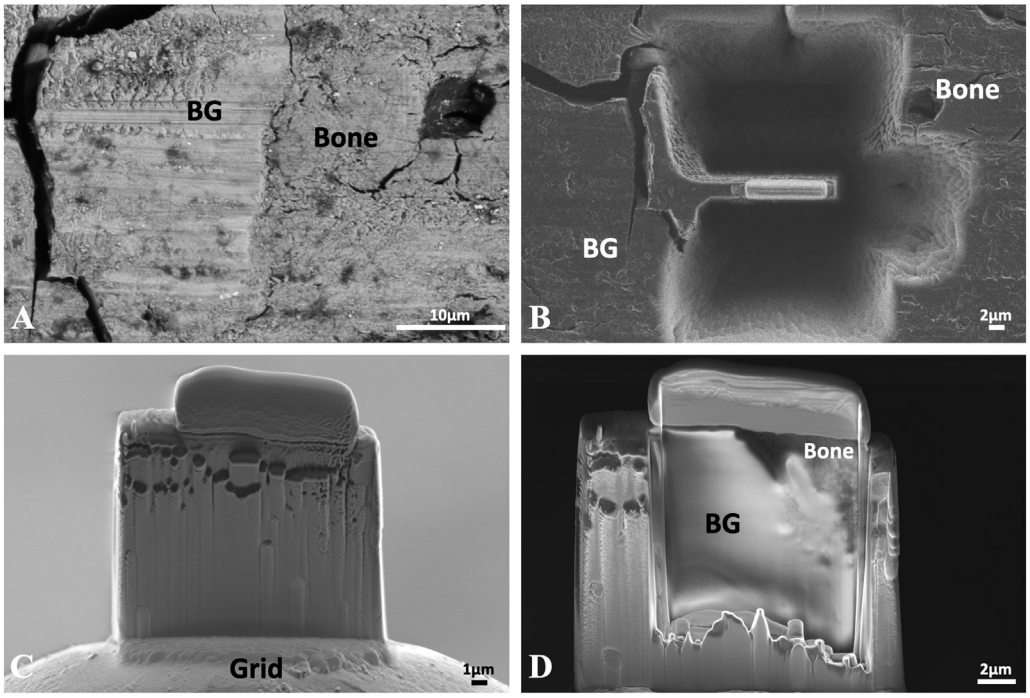

Fig. 1. The FIB lift-out procedure for preparing TEM samples illustrated for the ORQ BG group. A BSE-SEM image of the biomaterial (BG) and bone interface of interest for TEM sample preparation by FIB, including B trenches cut on both sides of the area of interest, protected by tungsten deposition; C the sample is attached to the TEM grid; D thinning of the sample by the ion beam.

endogenous peroxidase, 3% hydrogen peroxide (Merck Laboratories) was used. Antigen was retrieved by immersing the slices in citrate phosphate buffer, pH = 6, maintained in warm humidity, for 20 min. The non-specific reaction was blocked with bovine albumin (Sigma). The primary antibody used was against TRAP, whereas these polyclonal antibodies are produced in goats (Santa Crua Biotechnology). As the secondary antibody, rabbit anti-goat (Pierce Biotechnology) was used, and the amplifiers were avidin and biotin (Vector Laboratories) and chromogen to diaminobenzidine (Dako).

Immunolabeling analysis was performed through scores attribution, according to the area of positive presence of the proteins in the repairing tissue (interest area). For 25% of positive immunolabeling, it will be attributed the score 1; for 50% score 2; and for 75% score 3.

The objective of the immunostaining analysis was to characterize the osteoclastic activity in the different groups.

2.11. Statistical analyses

Statistical analyses were completed using the GraphPad Prism 8.1.1 software (GraphPadSoftware, La Jolla, USA). The analysis of homoscedasticity was performed by the Shapiro-Wilk test. One-way ANOVA was used to evaluate biomechanics, the parameters evaluated by micro-CT (BV/TV, Tb.Th, Tb.Sp, Tb.N, BIC), and MAR and NBA assessed by confocal laser microscopy regarding the measurement of overlapping fluorochromes, and when necessary, the Tukey's post-hoc test was applied. Two-way ANOVA was used to analyze the fluorochrome area. Significance level was set at $\alpha = 0.05$.

3. Results

The numerical values referring to the results of the present study are summarized in Table 2, and are described in more detail below.

3.1. Biomechanical analysis

The values of reverse torque obtained for each group are represented in Fig. 2. The maximum reverse torque necessary to remove the implants was the highest in SHAM BGPTH and SHAM BG groups with values of 9.6 N.cm and 8.2 N.cm respectively, followed by the ORQ BGPTH group with 6 N.cm. SHAM CLOT, ORQ BG and ORQ CLOT showed the lowest results with a reverse torque of 5.8 N.cm, 4.4 N.cm and 3 N.cm, respectively. However, the difference in reverse torque was not statistically significant for ORQ BGPTH with respect to SHAM BG ($p > 0.05$). On the contrary, the difference between SHAM BG and ORQ BG was statistically significant ($p < 0.05$).

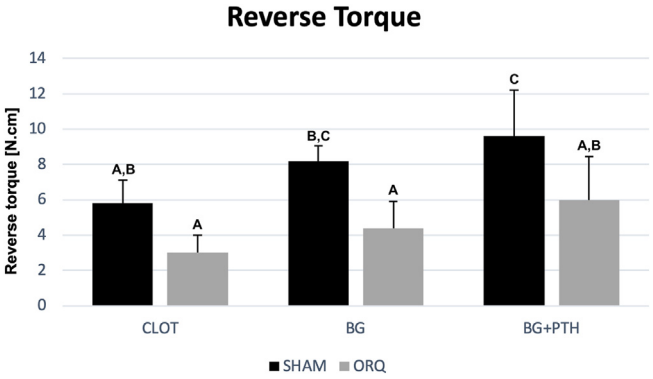

Fig. 2. Reverse torque values for the SHAM and ORQ groups evaluated for defects filled with clot only (CLOT), with Biogran® (BG) and Biogran® functionalized with PTH (BGPTH). Different letters denote statistical significance ($p < 0.05$).

3.2. Micro-CT

From the micro-CT measurements, the percentage of bone volume (BV/TV) (Fig. 3A) for the SHAM group was 64.40%, 60.22% and 29.79% for BGPTH, BG and CLOT groups, respectively. For the ORQ group, the highest bone percentage was present in the BGPTH group (60.32%), while the use of pure Biogran® (*i.e.* not functionalized with PTH) was able to form 50.37% of bone in the peri-implant defect, compared to the control ORQ CLOT group with only 27.57% BV/TV (SHAM and ORQ CLOT x SHAM and ORQ BG/BGPTH, one-way ANOVA, $p > 0.05$).

Regarding peri-implant bone trabeculae, trabecular thickness (Tb.Th) showed comparable results for all groups, with values ranging from 0.098 mm (ORQ CLOT) to 0.1133 mm (SHAM BGPTH), but without any statistical significance between groups (one-way ANOVA, $p > 0.05$) (Fig. 3B). Trabecular separation (Tb.Sp) displayed analogous values in the SHAM BGPTH (0.1 mm) SHAM BG (0.098 mm), ORQ BGPTH (0.1 mm) and ORQ BG (0.097 mm) groups, and a statistically significant (Tukey, $p < 0.05$) reduction in Tb.Sp was observed compared to the SHAM CLOT (0.1303 mm) and ORQ CLOT (0.135 mm) groups (Fig. 3C). As for the trabecular number (Tb.N), an average of 2.798/mm and 3.483/mm was obtained for the ORQ CLOT and SHAM CLOT groups, respectively, which was lower when compared to ORQ BG (5.345/mm), SHAM BG (5.45/mm), ORQ BGPTH (5.255/mm) and ORQ BG (5.651/mm) (Tukey, $p < 0.05$) (Fig. 3D).

As for the intersection between bone and implant, that is, the bone-implant contact (BIC), a larger three-dimensional contact area was identified for the BGPTH group for both SHAM (21.93 mm^2) and ORQ (18.93 mm^2) groups, but this difference was not statistically significant (Tukey, p

Table 2
Animal sample results: Control (SHAM) and orchiectomized rats (ORQ) - using clot (CLOT), Biogran® (BG) or Biogran® functionalized with PTH [1–34] (BGPTH) ± standard deviation (SD).

	SHAM			ORQ		
	CLOT	BG	BGPTH	CLOT	BG	BGPTH
Biomechanical	$n = 8$	$n = 8$	$n = 8$	$n = 8$	$n = 8$	$n = 8$
Reverse Torque	5.8 ± 1.3	8.2 ± 0.83	9.6 ± 2.6	3 ± 1	4.4 ± 1.51	6 ± 2.6
Bone structure	$n = 8$	$n = 8$	$n = 8$	$n = 8$	$n = 8$	$n = 8$
BV/TV (%)	29.79 ± 12.78	60.23 ± 5.78	64.33 ± 9.84	27.58 ± 2.01	50.38 ± 6.48	60.33 ± 5.48
Tb.Th (mm)	0.102 ± 0.019	0.110 ± 0.002	0.113 ± 0.009	0.098 ± 0.006	0.100 ± 0.009	0.107 ± 0.005
Tb.Sp (mm)	0.130 ± 0.015	0.098 ± 0.004	0.1 ± 0.014	0.135 ± 0.005	0.097 ± 0.008	0.100 ± 0.003
Tb.N (1/mm)	3.48 ± 1.39	5.45 ± 0.45	5.65 ± 0.53	2.79 ± 0.29	5.34 ± 0.48	5.25 ± 0.52
BIC - i.S (mm^2)	12.18 ± 1.08	15.67 ± 2.57	21.93 ± 1.85	10.79 ± 1.075	12.37 ± 2.99	18.93 ± 1.44
Bone dynamics	$n = 8$	$n = 8$	$n = 8$	$n = 8$	$n = 8$	$n = 8$
Fluorochrome (μm^2) Calcein/Alizarin	10,904 ± 1821	16,955 ± 4916	18,229 ± 6972	3178 ± 1900	100,068 ± 2097	13,949 ± 2258
MAR (μm/day)	1.67 ± 0.21	3.63 ± 0.28	3.94 ± 0.42	1.07 ± 0.19	2.48 ± 0.47	3.08 ± 0.32
NBA (μm^2)	8689 ± 3449	23,923 ± 3381	25,107 ± 4338	3299 ± 1163	15,953 ± 3841	21,194 ± 3280

BV/TV = percent bone volume; Tb.Th = trabecular thickness; Tb.N = trabecular number; Tb.Sp = trabecular separation; BIC = bone implant contact; i.S = intersection surface; MAR = mineral apposition rate; NBA = neoformed bone area.

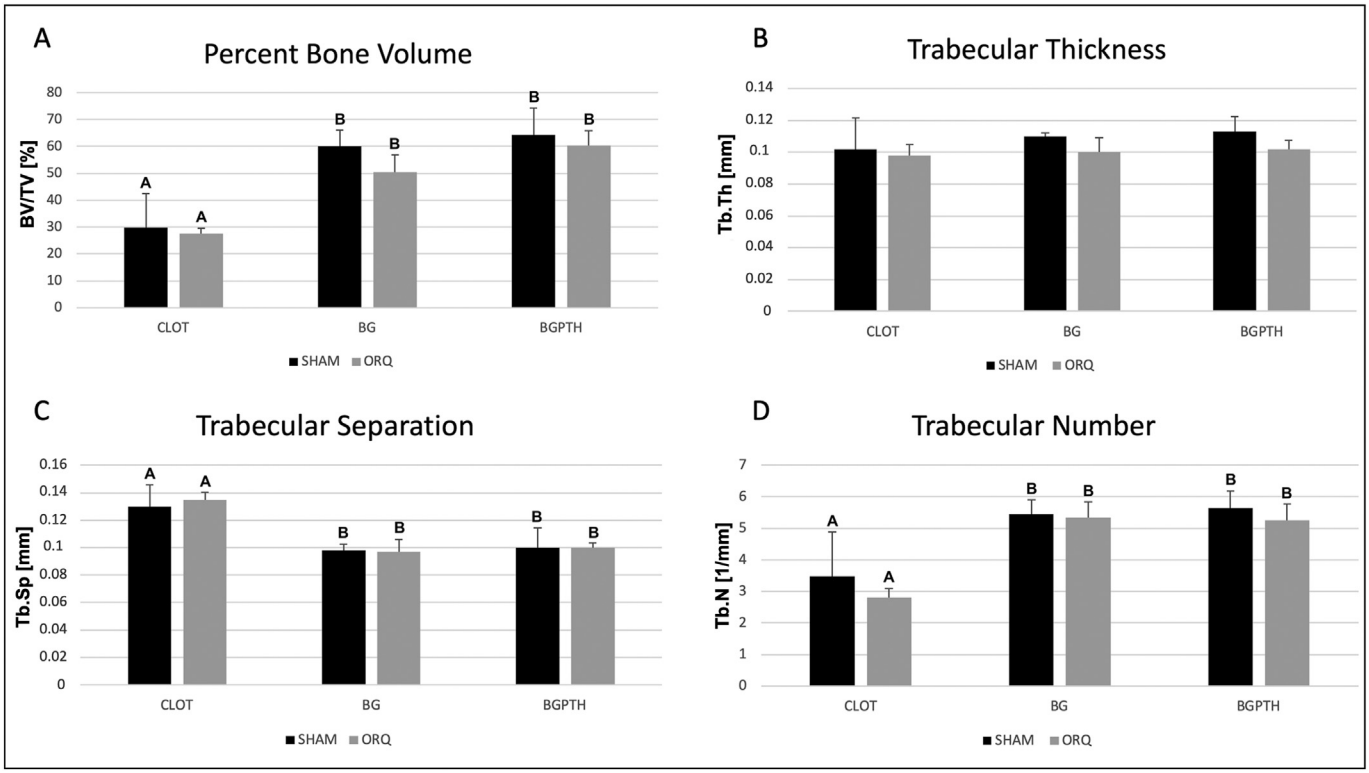

Fig. 3. Micro-CT analyses. A Percentage of bone volume (BV/TV). BG and BGPTH groups showed a higher BV/TV compared to CLOT group, both for SHAM and ORQ animals (different letters indicate $p < 0.05$); B Trabecular thickness (Tb.Th). All the groups displayed comparable values of Tb.Th (ANOVA, $p > 0.05$); C Trabecular separation (Tb.Sp). Higher values of Tb.Sp were obtained for SHAM CLOT and ORQ CLOT groups compared to SHAM BG, SHAM BGPTH, ORQ BG and ORQ BGPTH groups (different letters indicate $p < 0.05$); D Trabecular number (Tb.N). Lower values of Tb.N were observed for SHAM CLOT and ORQ CLOT groups compared to SHAM BG, SHAM BGPTH, ORQ BG and ORQ BGPTH groups (different letters indicate $p < 0.05$).

> 0.05). However, the difference in BIC in the ORQ BGPTH and SHAM BG groups was also not statistically significant (Tukey, $p > 0.05$), suggesting that the peri-implant defect of the osteoporotic animal filled with PTH-functionalized biomaterial had the same reparational behavior as the healthy animal treated with biomaterial only (Fig. 4). A representative three-dimensional rendering of the bone present around the implant is provided for each group in Fig. 5.

3.3. Confocal laser microscopy

The fluorochromes calcein (green) and alizarin (red) served to mark the calcium matrix, thus demonstrating the dynamics of peri-implant bone repair in all the experimental groups (Fig. 6). This allowed for assessment of bone dynamics, including total area, daily calcium depositions or mineral apposition rate (MAR), and neoformed bone area (NBA).

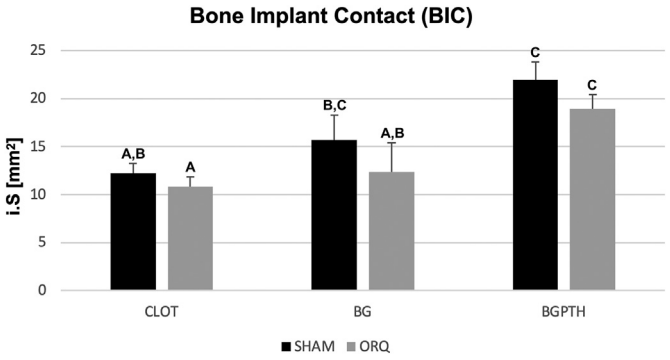

Fig. 4. Values of bone-implant contact (BIC) evaluated from micro-CT analysis. Different letters represent statistical significance ($p < 0.05$). There is no statistical difference between ORQ BGPTH and SHAM BG, suggesting PTH in ORQ has the same reparational capacity as healthy bone with biomaterial alone.

In the intragroup evaluation of the fluorochromes area in green and red, no statistically significant difference was found (two-way ANOVA, $p > 0.05$). In the intergroup comparison, the average of the results obtained showed the highest numerical result for the SHAM BGPTH group, being statistically significant in comparison with the other groups (Tukey, $p < 0.05$). SHAM BG and ORQ BGPTH displayed similar results in terms of fluorochromes area (Tukey, $p > 0.05$), indicating that the functionalization of Biogran® with PTH 1–34 in osteoporotic rats allowed for comparable repair of peri-implant defects as in healthy animals that received non-functionalized Biogran® (Fig. 7A). This was further supported by the evaluation of new bone formation, as the value of NBA for the ORQ BGPTH group was comparable to that of the SHAM BG and SHAM BGPTH groups (Tukey, $p > 0.05$) (Fig. 7B).

Daily mineral apposition ranged from 1.07 μm (ORQ CLOT) to 3.94 μm (SHAM BGPTH). The results (Fig. 7C) were: SHAM: 1.67 μm (CLOT), 3.62 μm (BG) and 3.94 μm (BGPTH); and for ORQ: 1.07 μm (CLOT), 2.48 μm (BG) and 3.08 μm (BGPTH). Similarly to fluorochrome area, topical PTH led to an increase in daily mineral apposition in osteoporotic animals (ORQ BGPTH group), showing no statistically significant difference when compared to SHAM BG (Tukey, $p < 0.05$).

3.4. RT-PCR

For all parameters evaluated with RT-PCR, the SHAM CLOT group was considered the standard, receiving a fixed value of 1, thus the other groups were evaluated with respect to this reference. The relative expression of ALP for the ORQ BG (0.808), SHAM BG (1.118) and SHAM BGPTH (1.451) groups did not show a statistically significant difference when

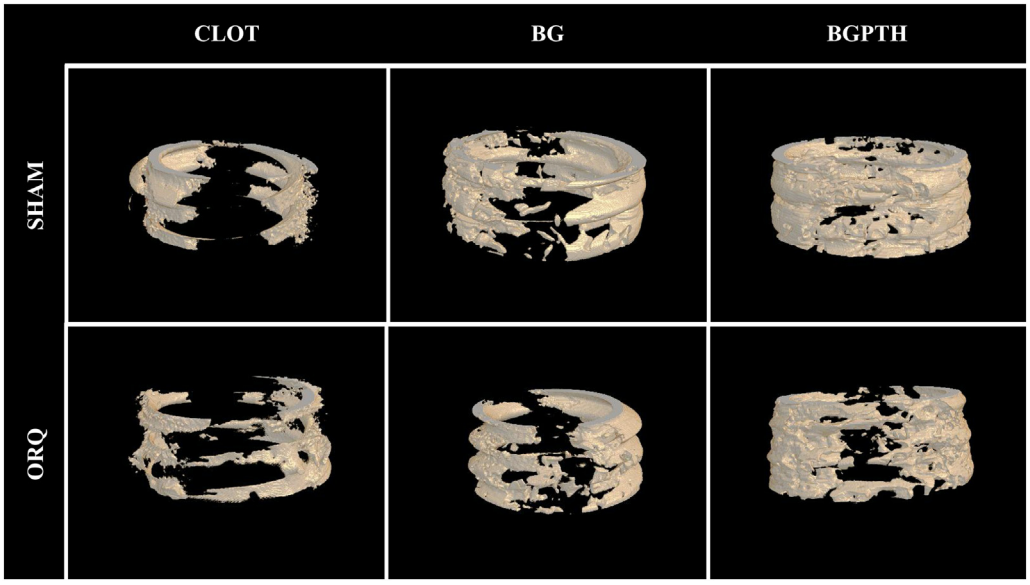

Fig. 5. Three-dimensional rendering of the bone formed around the implant threads in the different experimental groups obtained from micro-CT.

compared with SHAM CLOT (reference value 1.0). The ORQ CLOT group had the lowest value for ALP expression (0.33), which was statistically significant with respect to the SHAM CLOT group (Tukey, $p = 0.01$). The highest ALP expression was found for the ORQ BGPTH group (6.044), a result that was statistically significant compared to all the other groups (Tukey, $p < 0.05$) (Fig. 8A).

The relative expression of OC was similar for the SHAM CLOT (1.0), SHAM BG (1.283), SHAM BGPTH (1.706), ORQ BG (1.569) and ORQ BGPTH (1.489) groups, and no statistically significant difference between the groups was identified (ANOVA, $p > 0.05$). The ORQ CLOT group displayed the lowest value of OC expression, which was statistically significant compared to the ORQ BG, ORQ BGPTH and SHAM BGPTH groups (Tukey, $p < 0.05$) (Fig. 8B).

3.5. Elemental and ultrastructural analysis

3.5.1. SEM and elemental analysis by EDS

SEM images of the bone-Biogran® interface and EDS maps of Biogran® particles after 30 days *in vivo* revealed an uneven elemental distribution with Ca/P highly concentrated towards the particle exterior and a Si-rich core (Fig. 9). EDS analysis was performed on BG and BGPTH groups, with one representative map and extracted elemental profile given for SHAM (Fig. 10) and ORQ (Fig. 11) groups. While these images and elemental profiles are not compared statistically, there are some common observations to draw. The SHAM BG and BGPTH groups showed a very low (almost absent) amount of Si at the extremities, which were predominantly of Ca and P, and very high (approximately 3.5× more than Ca and P) amount in the central

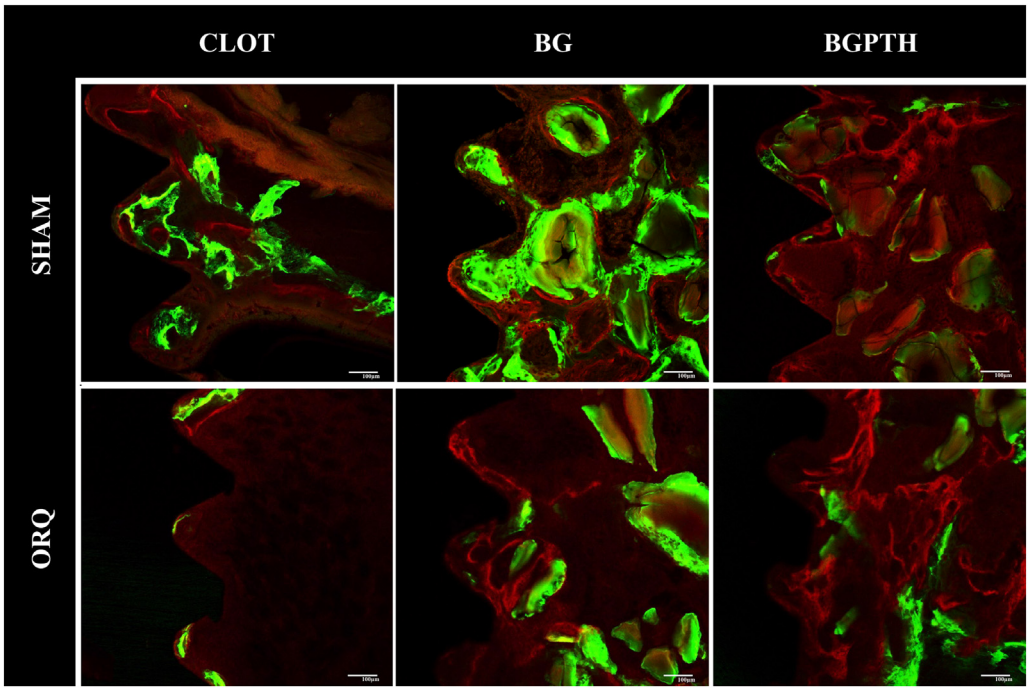

Fig. 6. Calcein (green) and alizarin (red) marking the calcium matrix, demonstrating the dynamics of the peri-implant bone of the experimental groups.

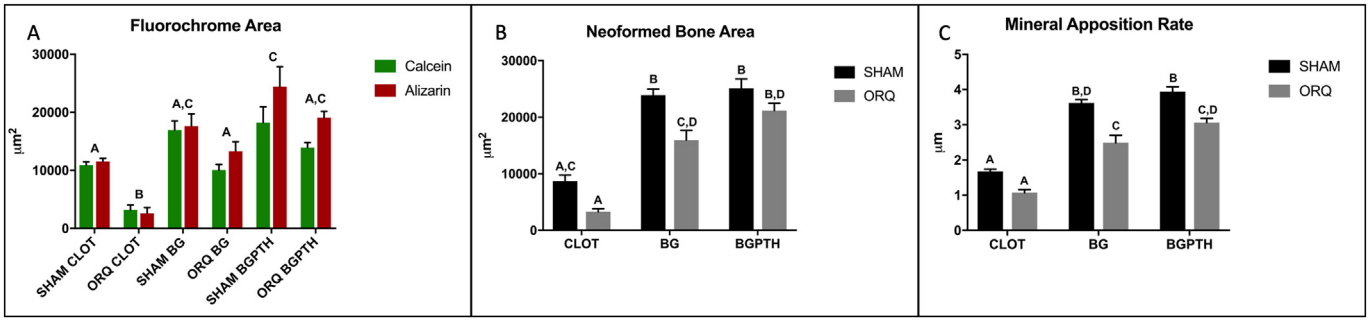

Fig. 7. Fluorochrome analyses across all groups: SHAM and ORQ in the different CLOT, BG and BGPTH groups. A Quantification of the fluorochrome area calcein (green) and alizarin (red), where SHAM BG shows similarity to ORQ BGPTH. B Values referring to neoformed bone area (NBA), where ORQ BGPTH shows no statistical difference from SHAM BG and SHAM BGPTH. C Values referring to the bone mineral apposition rate (MAR), which similar to fluorochrome area showed no difference between ORQ BGPTH and SHAM BG. Different letters denote statistical significance ($p < 0.05$).

region of the biomaterial. In addition, Si was present an average of 200 µm across each 300 µm particle imaged for both groups (Fig. 10B and D). Similarly, the ORQ groups showed amounts of Si in the interior nearly double when compared to Ca and P on the exterior (Fig. 11B and D). However, in the case of these 300 µm particles, the Si inside the particle extended only about 100 µm (Fig. 11B and D).

3.5.2. Scanning transmission electron microscopy

HAADF-STEM imaging showed the connection between bone and biomaterial at the nanoscale, allowing to understand whether there is a structural gradient or interfacial zone between the bone and the biomaterial. In all groups an intimate connection at the nanoscale level between newly formed bone and Biogran® was present (Figs. 12-15). Often, the interface,

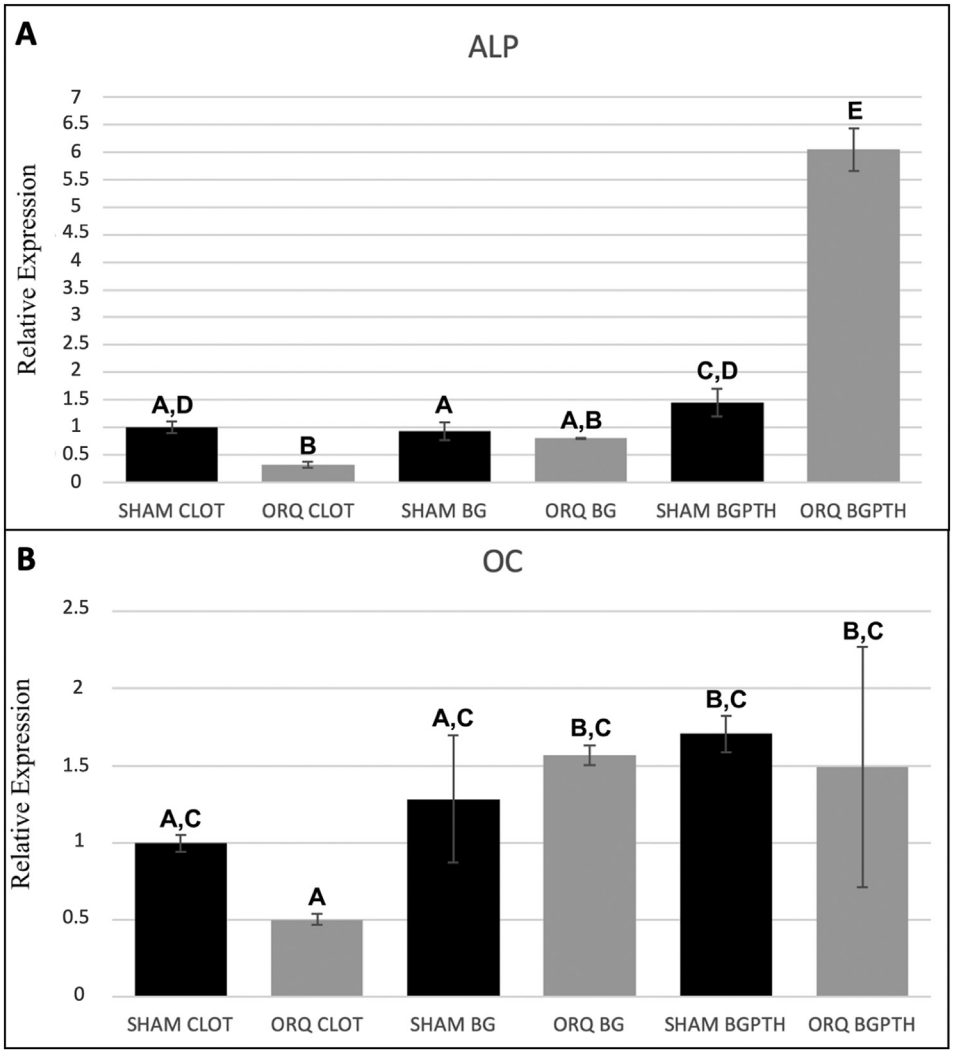

Fig. 8. Relative gene expression of ALP (A) and OC (B) in the period of 60 days in the CLOT, BG and BGPTH groups, both SHAM and ORQ. The highest relative expression of ALP was found for ORQ BGPTH, while OC expression was statistically lower in ORQ CLOT than both ORQ BG and ORQ BGPTH. Different letters indicate statistical significance ($p < 0.05$).

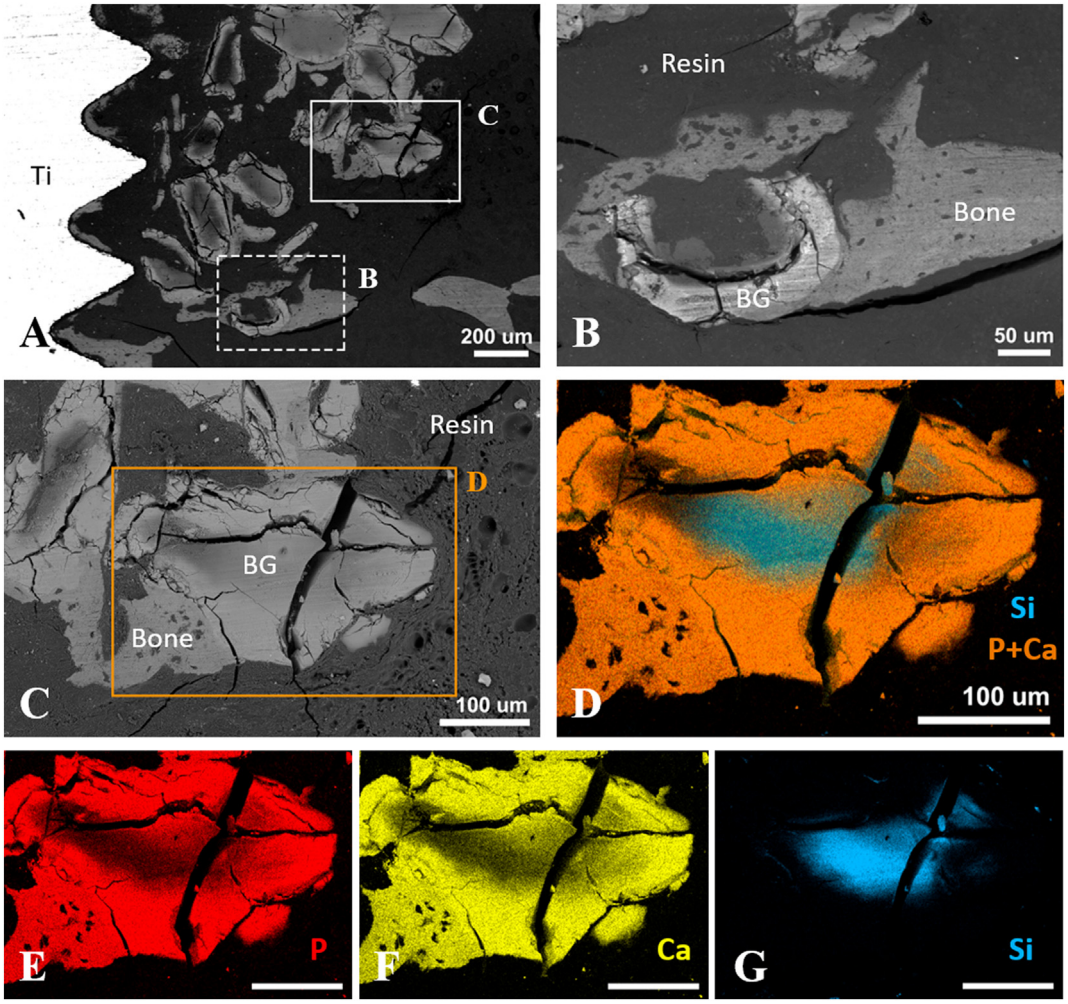

Fig. 9. A,B BSE-SEM image of the biomaterial and bone interface and C a representative Biogran® particle (BG) with D Elemental mapping by EDS showing a high exterior concentration of Ca and P (orange) and Si (blue) rich core. E,F,G Discrete elemental maps for P (red), Ca (yellow) and Si (blue) shown separately. Scale bar = 100 μm.

or better, the interphase, between bone and Biogran® appeared gradual and it ranged from 150 nm to up to 700 nm in thickness in the regions examined. In all samples, collagen fibres in the newly formed bone appeared to be laid down parallel to the Biogran® interface. In addition, new bone displayed a rather immature structure, as expected from the early retrieval time point (30 days). More organized collagen fibres could be distinguished in the ORQ groups, especially with PTH-functionalized Biogran®, for which the collagen banding pattern was more visible.

In the SHAM BG group (Fig. 12), an external dissolution/reprecipitation of the biomaterial was observed, which presented an average interphase of 150 nm. In addition, dissolution towards the inner part of the Biogran® particle, with almost total separation of a segment of the particle, was observed. Within this area, a greater dissolution zone of approximately 300 nm was found, in addition to an area resembling new bone formation (marked by *). Similarly, the SHAM BGPTH group (Fig. 13) showed an area of external dissolution/reprecipitation approximately 350 nm in width (Fig. 13D) and the same immature bone as the BG group, but with clear collagen banding at the interface. However, no area of internal dissolution of the biomaterial was noted in this individual particle.

For the ORQ BG group (Fig. 14), there was presence of bone that was still immature, but distinct mineral clusters were visible in some regions (Fig. 14B) while organized collagen fibrils, distinguishable due to their alignment in the plane of the image, were visible in other regions (Fig. 14D). As in other groups, the dissolution present was irregular and approximately 180 nm in width, and again without the presence of dissolution in internal cavities of the particle.

In the ORQ BGPTH group (Fig. 15), it was possible to observe a linear area in the most superficial portion of the particle with dissolution of the biomaterial underway up to approximately 770 nm in width (Fig. 15C). Underneath this, a greater dissolution area into a cavity towards the interior of the particle was visible. In this cavity showing 900 nm of dissolution (Fig. 15E), it was possible to observe the presence of an area with new bone formation (Fig. 15D,E,F marked by *). The bone juxtaposed to the exterior of the sample was in close contact with the particle and had distinct organized collagen bands visible, which were parallel to the biomaterial, suggesting greater bone organization. However, this could be simply related to the collagen fibrils being at an optimal orientation for imaging.

3.6. Immunohistochemical analysis

TRAP immunolabeling was performed in order to characterize osteoclastic activity during the peri-implant repair in the different conditions evaluated in the present study.

TRAP is a marker of an enzyme that is present in osteoclasts, during their activity. The images were captured in the area of medullary bone, the region of interest in the model of tibia's implants installation, exception on orchiectomy clot group when the image represents the cortical bone just in order to characterize the aspect of the osteoclasts in the activity, present in bone areas close to the implant.

One aspect that is observed is that in all of the groups evaluated in this study, there was a gap that was around the implant, causing an

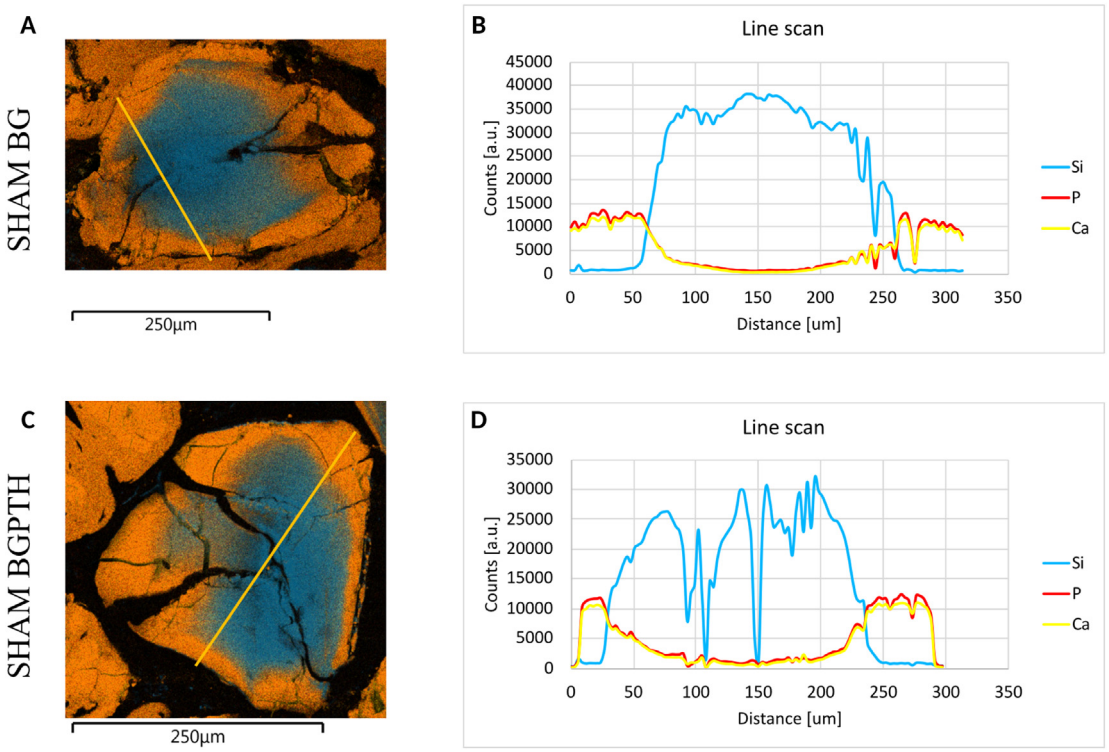

Fig. 10. A,C: Elemental maps of the biomaterial of the SHAM BG and BGPTH groups showing a predominance of Si (blue) inside the particle and Ca and P (orange) at the periphery; B,D: Elemental line profiles of the biomaterial particle showing a relative predominance of Si in the core, nearly 3.5× higher than Ca and P measured at the periphery.

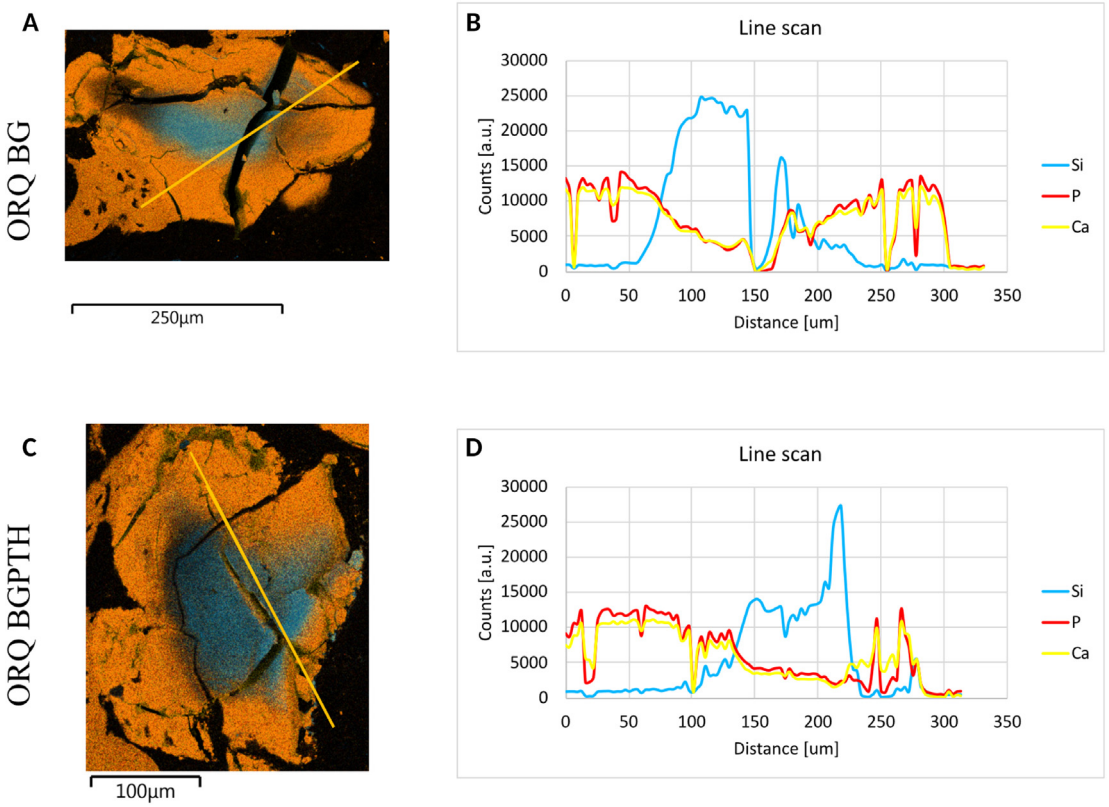

Fig. 11. A,C: Elemental maps of the biomaterial of the ORQ BG and BGPTH groups showing a predominance of Si (blue) inside the particle and Ca and P (orange) at the periphery; B,D: Elemental line profiles of the biomaterial particle showing a Si-rich core that spans only about 100 μm.

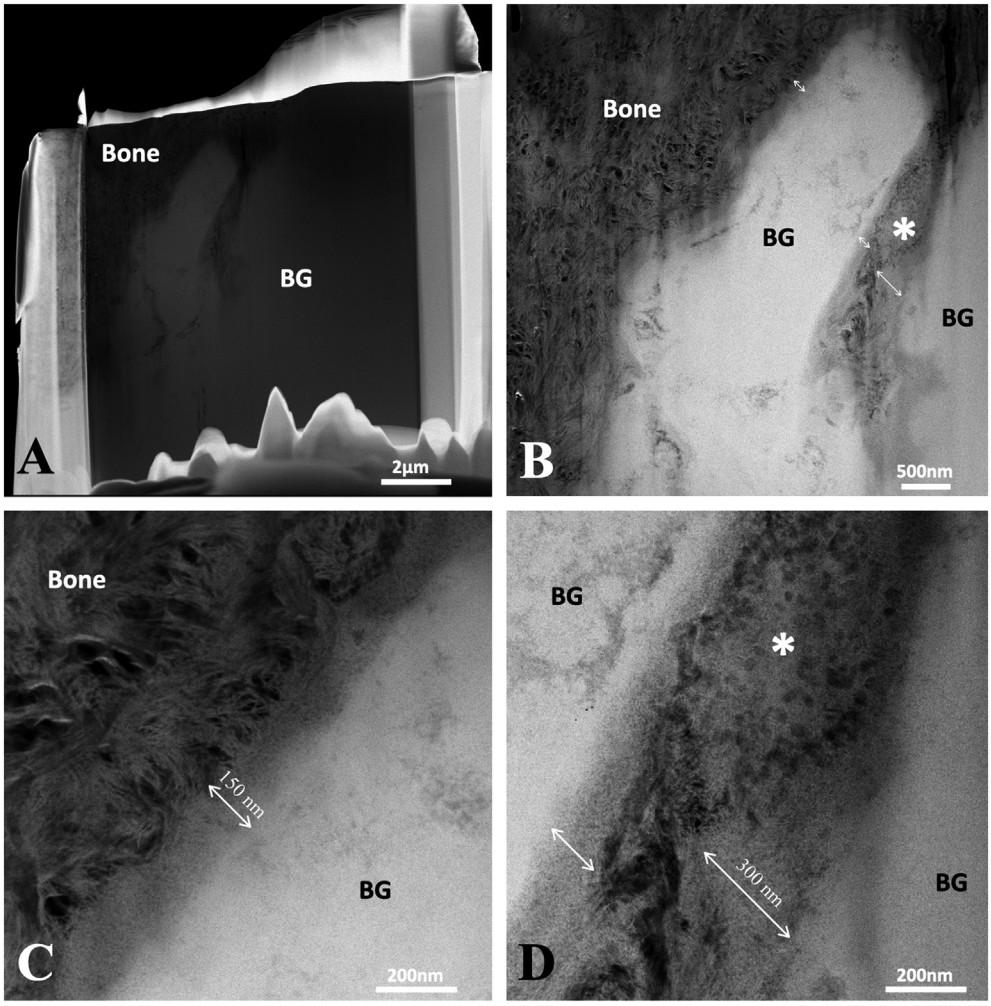

Fig. 12. Ultrastructural analyses from the SHAM BG group; A: Overview image of the entire sample as prepared in the FIB; B, C, D: STEM-HAADF images with different magnifications of the bone-biomaterial interface. A small cavity with bone ingrowth is noted in B and D by *,while the surface-active Ca/P layer is marked by double ended arrows in C and D. (BG = Biogran®; * = Region of new bone formation).

impairment of the adjusts of the implant in the preparation bed. In groups BG and BGPTH, the gap was filled for these biomaterials, in order to improve the adjustment between the implant and the preparation bed.

In SHAM group, it was observed that in the clot group, there isn't a the medullar region with a poor quantity of bone formed close to the implant's threads (negative area of the image), with discrete labeling for osteoclasts. When BG was used to fill the gap, it was observed that in the medullar region, bone was formed close to the implant's threads and a discrete to moderate labeling for osteoclasts was observed in the area. When PTH was added to BG, the formation of bone close to the implant's threads was also observed as well as a discrete to moderate positive labeling for osteoclasts.

When orchiectomy was performed in the animals what represents a challenge for the peri-implant repair process, it was possible to highlight that in the clot group, there was positive labeling for TRAP, in a discrete manner, but we consider that is a response for the osteopenia caused by the systemic condition. Note that the representation is for cortical bone, just in order to illustrate the aspect of the trap positive labeling and the aspect of the osteoclasts that are labeling in cortical bone, close to the implants. When BG was used to fill the gap, it was observed a discrete to moderate labeling of trap in osteoclasts and in BGPTH it was observed moderate labeling of osteoclasts (Fig. 16).

4. Discussion

Animals subjected to orchiectomy develop osteoporosis as a consequence of the sudden decrease in endogenous testosterone caused by this surgical procedure, as testosterone is directly related to bone formation. In addition, there are indications that aromatization of testosterone to estradiol plays an important role in the regulation of bone homeostasis in men [21,28,40]. Therefore, there will be a decrease in bone formation and a likely increase in bone resorption, ultimately leading to a rapid onset of osteoporosis after orchiectomy.

Biogran® is a commercially available bone graft used in dentistry [41,42]. Previous work has reported the functionalization of Biogran® with Raloxifene®, a selective estrogen receptor modulator, using sonochemistry [5,28]. The sonochemical method relies on the phenomenon of acoustic cavitation, *i.e.*, the formation, growth and implosive collapse of bubbles in liquids with time in the order of microseconds, to mix two or more distinct substances [5]. Sonochemistry was chosen for the functionalization of the biomaterial proposed in the present work because it enables the modification of a wide variety of nanostructured materials from ultrasonic waves in a liquid medium, which cause chemical and physical transformations in the sample. Moreover, it is an economical and effective method to reduce and homogenize the size of particles due to the application of high pressures in a short time, inducing a rapid morphological change [28,43]. In this work, sonochemistry was used to homogenize Biogran® particles

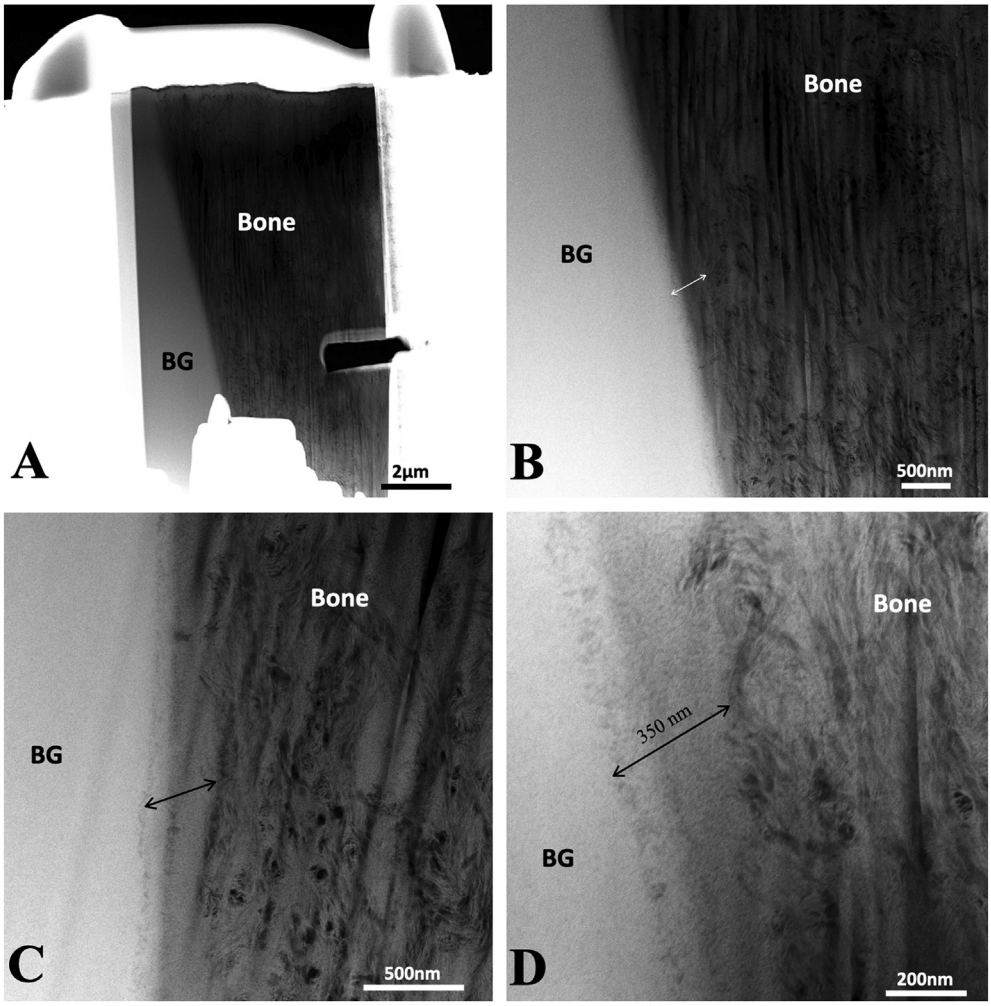

Fig. 13. Ultrastructural analyses from the SHAM BGPTH group; A: Overview image of the entire sample as prepared in the FIB; B, C, D: STEM-HAADF images with increasing magnifications of the bone-biomaterial interface. Double ended arrows mark the dissolution/reprecipitation bioactive layer visible on the surface. (BG = Biogran®).

and to functionalize them with PTH 1–34, an anabolic drug that acts directly on the WNT pathway, thereby signaling the formation of bone tissue [26]. Sonochemistry was carried out for 15 min, which was identified as an optimal time for the PTH functionalization of Biogran® in a previous study [26].

The implant/bone-graft/bone interface is a complex repair situation, which involves revascularization, graft incorporation and implant integration [44]. The combination of biomaterials as synthetic bone grafts with implants has been studied and used frequently in cases of post-exodontics peri-implant defects and bone fenestrations [44]. The osteoconductive properties of biomaterials and the physicochemical processes occurring *in vivo* after implantation are fundamental for bone repair. Biogran® is a silica-based bioactive glass, with demonstrated osteoconductivity, made of SiO_2(45 wt%), CaO (24.5 wt%), Na_2O (24.5 wt%) and P_2O_5 (6 wt%) [3]. After contact with body fluids, silica-rich bioactive glasses undergo an interfacial ion exchange, in which Si is rapidly released from the surface [illegible] and PO_4^{3-} from the material and external environment to form a gel of CaO–P_2O_5 on the silica-rich layer which then crystallizes with incorporation of hydroxyls and carbonates from solution and forms a surface layer of hydroxyapatite [45]. Such bioactive surface layers were noted herein on all groups by STEM imaging (Figs. 12-15). With increasing time, phagocytosing cells begin the resorption of these layers and, after this resorption, mesenchymal cells penetrate small ducts and adhere to the CaP layer formed more internally, where they are differentiated into osteoblasts and initiate the bone formation process inside the biomaterial even if there is no presence of previous bone at the site [3]. Indication of such internal formation of bone in Biogran® cavities was noted randomly in some samples, including SHAM BG and ORQ BGPTH, in Fig. 12 and Fig. 15.

The creation of a CaP-rich outer layer and a Si-rich core was shown in previous EDS line scans across Biogran® particles implanted in the edentulous jaws of beagle dogs [4]. In this study, EDS mapping of Biogran® verified the presence of a core richer in Si and an outer surface more concentrated in Ca and P. Notably, such distribution pattern of Ca, P and Si was analogous for particles functionalized by PTH 1–34 and for those implanted in osteoporotic animals, suggesting that neither the presence of PTH locally, nor the different metabolism in osteoporotic bone altered the characteristic interfacial ion exchange of Biogran® *in vivo*. However, for ORQ BG and ORQ BGPTH this process seemed to be slightly more accentuated and the ion exchange intensified since the layer of Ca and P in the periphery of the biomaterial was larger than that of Si inside the particle. Since only a few particles were probed herein, whether or not the rate of dissolution of Si into the surrounding environment is higher in ORQ groups requires further investigation, but it is plausible that local changes in pH would affect this rate.

This bioactive surface layer associated with Biogran® contributes to its osteoconduction and therefore, the quantity and quality of new bone formation surrounding an implant as well as its biomechanical strength when used in peri-implant bone graft applications. Biomechanical analysis of the bone-implant interface (Fig. 2) revealed that in each subgroup (CLOT, BG and BGPTH) smaller values of reverse removal torque were registered in the ORQ group than in the SHAM one, in turn indicating that the

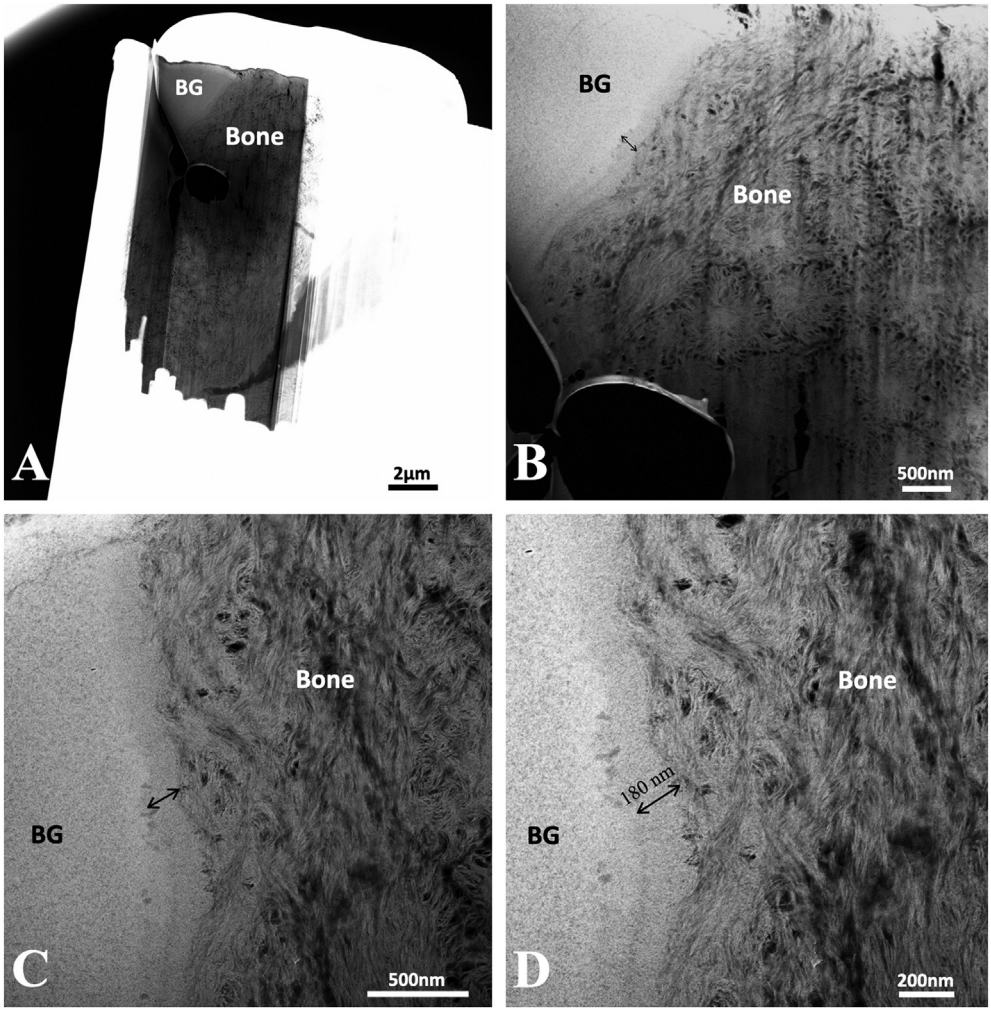

Fig. 14. Ultrastructural analyses from the ORQ BG group; A: Overview image of the entire sample as prepared in the FIB; B, C, D: STEM-HAADF images with different magnifications of a few regions at the bone-biomaterial interface. Double ended arrows mark the dissolution/reprecipitation bioactive layer visible on the surface. Under the label, "bone" in B, mineral clusters in newly deposited bone are visible, while C and D show alignment of collagen fibrils parallel to the interface, marked by collagen banding. (BG = Biogran®).

level of osseointegration was lower in the osteoporotic animals than in the healthy ones. Interestingly, no statistically significant difference in reverse torque was observed when comparing the healthy animal that received Biogran® only (SHAM BG) to the osteoporotic animal that received Biogran® functionalized with PTH 1–34 (ORQ BGPTH). This suggests that the topical application of PTH can improve the biomechanical stability of osseointegration in presence of osteoporosis, reaching a comparable level as that achieved using non-functionalized Biogran® in healthy skeletal conditions, which is promising for clinical dental applications.

This reverse torque result can be directly related to the results of BIC evaluated from micro-CT (Fig. 4 and Fig. 5), which shows that SHAM BG, SHAM BGPTH and ORQ BGPTH displayed the highest values of BIC, with no statistically significant difference among each other. This seems to indicate that, while the functionalization with PTH 1–34 does not have a significant effect in healthy animals, it plays a role when osteoporosis is present, as BIC was higher in the ORQ BGPTH group compared to ORQ BG. Similar results were found previously in the case of systemic administration of PTH 1–34 in orchiectomized rats, where an improvement in BIC was achieved compared to untreated animals, both osteoporotic and healthy [33].

Other micro-CT evaluation of the samples (Fig. 3) showed statistically significant differences in bone volume, trabecular separation and trabecular number only when comparing groups with biomaterial with or without functionalization (SHAM BG, SHAM BGPTH, ORQ BG, ORQ BGPTH) in relation to groups filled with clot only (SHAM-CLOT, ORQ-CLOT), indicating the reparative role that inclusion of the Biogran® itself plays on bone formation.

An aspect of fundamental importance to be evaluated is the osteoclastic activity present in the peri-implant repair in the proposed model. The cellular morphology present in osteoclasts in the SHAM group are mononucleated macrophages, different from the ORQ groups in which they have mature osteoclasts, probably due to orchiectomy showing greater cell recruitment. The ORQ CLOT group was represented by cortical bone to illustrate how osteoclasts were in this region. In the ORQ BG group, the labeling TRAP is in mononuclear cells, due to bone remodeling activity in which active resorption has already passed. In the BGPTH groups, active osteoclasts are observed apparently due to the local action of parathyroid hormone, contributing to a better turnover in the region, acting positively to maintain an active bone and consequently improving its quality.

Values of MAR (Fig. 7) confirmed the trend observed in the measurements of reverse torque, *i.e.*, that ORQ BGPTH group did not show any statistically significant difference compared to SHAM BG, in turn indicating that the PTH functionalization leads to a peri-implant repair process for osteoporotic bone analogous to that of healthy bone. The contribution of PTH in making the repair level for osteoporotic and healthy bone comparable was also noticed in the fluorochrome (calcein and alizarin) area and NBA analyses, since there was no statistically significant difference in the mean values for the ORQ BGPTH, SHAM BG and SHAM BGPTH groups. The data of calcium precipitation and NBA suggest that topical PTH 1–34

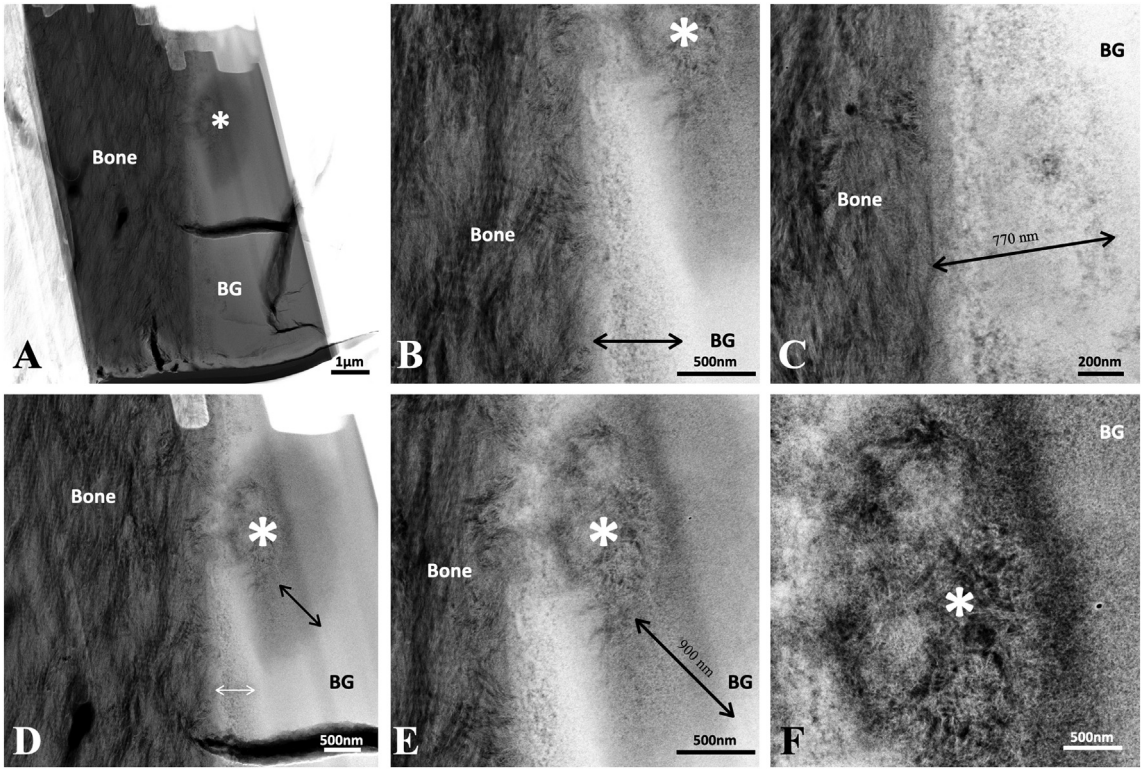

Fig. 15. Ultrastructural analyses from the ORQ BGPTH group; A: Overview image of the entire sample as prepared in the FIB; B, C: STEM-HAADF images with different magnifications of various regions along the bone-biomaterial interface, showing the bioactive surface layer marked by double ended arrows. D, E, F: STEM-HAADF images highlight an internal cavity where new bone ingrowth is noted by *, surrounded by a large dissolution/reprecipitation layer. (BG = Biogran®; * = Region of new bone formation).

contributes to making the process of new bone formation comparable in osteoporotic and healthy groups, while its effect in improving bone repair is not remarkable in healthy animals (SHAM BG and SHAM BGPTH). This is consistent with current clinical practices, where health individuals receive biomaterial only. This finding could be partly explained by RT-PCR results (Fig. 8), showing that the relative expression of ALP was much more elevated in the osteoporotic animals treated with functionalized Biogran® (ORQ BGPTH) compared to all the other groups, displaying a six-fold increase in ALP expression with respect to the reference group (SHAM CLOT). This may be indicative of a higher local bone activity, in turn facilitating mineral deposition in these animals. The higher expression of ALP in the ORQ BGPTH animals could also explain the higher level of bone organization visible in HAADF-STEM images of this group, as opposed to a rather immature structure observed in the other groups. HAADF-STEM imaging

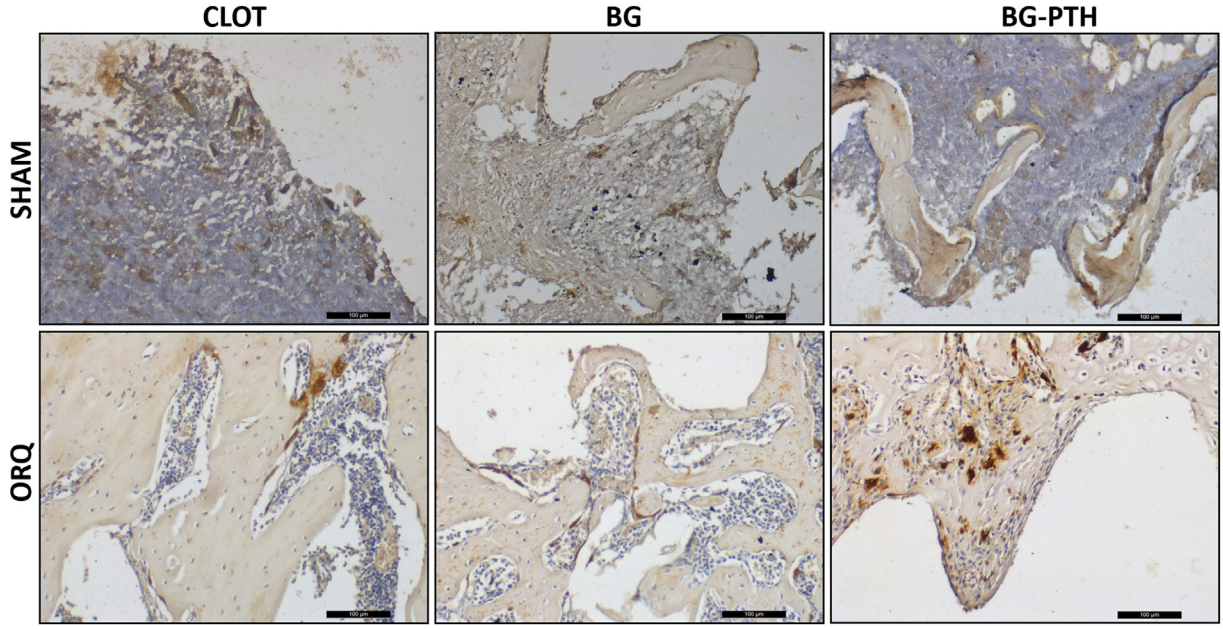

Fig. 16. Immunohistochemistry using proteins against TRAP. Immunolabeling of these proteins in SHAM and ORQ – CLOT, BG e BGPTH. Immunolabeling was defined as: mild; moderate and intense.

visualized the bone-Biogran® (without and with PTH 1–34) interface at the nanoscale, resolving the gradual layer where the biomaterial dissolves and apposition of Ca/P and subsequently new bone takes place. To our knowledge, this is the first time that the interfacial ion exchange process leading to bone repair in presence of Biogran® is visualized at the nanoscale. From this level of resolution of newly formed bone juxtaposed to Biogran®, it was possible to identify collagen fibrils oriented parallel to the interface, analogously to what observed for other ceramic biomaterials [46] or in case of titanium implants. Interestingly, a newly observed structure in bone, consisting of ellipsoidal mineral clusters [47], or circular features observed in cross-section called “rosettes” [48] are visible in both the ORQ groups. These clusters have been noted in early forming bone [49], as well as in fully developed, more mature bone of the human femoral neck [50]. To date, these have not been identified in osteoporotic bone, but are shown here to form after orchiectomy.

It is important to understand that the bone formation process around the biomaterial starts after the onset of the ion exchange of Ca/P and Si [3,51] at the biomaterial surface and cavities, and that PTH initiates cellular responses, one of which manifests in the activation of proteins from the extracellular matrix, such as ALP and OC expression. In the present work, ALP was expressed significantly more when topical PTH was used in orchiectomized rats (ORQ BGPTH) compared to the relative gene expression found in the other groups, which may lead the improvement in bone formation, since this protein is essential for the formation of quality bone tissue. The role of PTH in ALP expression *in vitro* has been well documented, where early osteoblast differentiation and ALP expression were improved with increasing PTH dose [50]. Similarly, in osteoporotic women receiving PTH systemically, all showed an increase in ALP expression over the first 6 months of treatment with PTH [52]. This correlation to *in vitro* and clinical systemic modes of delivery bolsters the unique findings herein that local delivery also impacts peri-implant bone repair.

5. Conclusion

Biogran® is a clinically available allograft used in the dental practice. For the first time, this work reports on the functionalization of Biogran® with PTH 1–34 using sonochemistry for local delivery in the peri-implant space. The local administration of this anabolic agent was shown to be beneficial for improving peri-implant bone repair in conditions of low bone quality and quantity, such as osteoporosis. This was confirmed in this study where orchiectomized rats that received Biogran® functionalized with PTH 1–34 showed similar results in terms of bone repair as healthy animals that received non-functionalized Biogran®. In particular, it appears that the topical action of PTH 1–34 led to an increased bone formation and local calcium precipitation, especially in orchiectomized animals. This can be attributed to the ability of PTH 1–34 to activate specific proteins in the extracellular matrix, in particular enhancing expression of ALP, which is fundamental for the formation of quality bone tissue. In view of these results, we conclude that it is essential to use biomaterials functionalized with PTH 1–34 to fill peri-implant defects in osteoporotic bone.

Declaration of competing interest

The authors declare that they have no known competing financial interests or personal relationships that could have appeared to influence the work reported in this paper.

Acknowledgments

Funding support is acknowledged from (FAPESP) for funding this work (process number: 2017/08187-3 and 2015/14688-0), CAPES (UNESP/CAPES/Print Project) Medens (implants used in the research), Multiuser laboratory of Araçatuba Dental School-UNESP and FINEP (FINEP/CT-INFRA – Covenant FINEP: 01.12.0530.00 PROINFRA 01/2011) and the Natural Science and Engineering Research Council of Canada (NSERC). RO is affiliated with the Research Productivity Scholarship (process no.: 306389/2017-7). Biogran sonochemistry and functionalization were carried out at the Advanced Materials Laboratory of the Centre for Research and Development of Functional Materials – Health Division – FAPESP (São Paulo, SP, Brazil), under direction of Prof. Paulo Noronha Lisboa-Filho. Electron microscopy work was completed at the Canadian Centre for Electron Microscopy (CCEM) at McMaster University.

References

[1] W.C. Stentz, B.L. Mealey, P.V. Nummikoski, J.C. Gunsolley, T.C. Waldrop, Effects of guided bone regeneration around commercially pure titanium and hydroxyapatite-coated dental implants. I. Radiographic analysis, J. Periodontol. 68 (3) (1997) 199–208.
[2] J.E. Davies, Understanding peri-implant endosseous healing, J. Dent. Educ. 67 (8) (2003) 932–949.
[3] E. Schepers, M. de Clercq, P. Ducheyne, R. Kempeneers, Bioactive glass particulate material as a filler for bone lesions, J. Oral Rehabil. 18 (5) (1991) 439–452.
[4] E.J. Schepers, P. Ducheyne, L. Barbier, S. Schepers, Bioactive glass particles of narrow size range: a new material for the repair of bone defects, Implant. Dent. 2 (3) (1993) 151–156.
[5] C. Chan, I. Thompson, P. Robinson, J. Wilson, L. Hench, Evaluation of Bioglass/dextran composite as a bone graft substitute, Int. J. Oral Maxillofac. Surg. 31 (1) (2002) 73–77.
[6] C.E. Misch, F. Dietsh, Bone-grafting materials in implant dentistry, Implant. Dent. 2 (3) (1993) 158–167.
[7] T. Furusawa, K. Mizunuma, Osteoconductive properties and efficacy of resorbable bioactive glass as a bone-grafting material, Implant. Dent. 6 (2) (1997) 93–101.
[8] K.C. Leung, T.W. Chow, P.Y. Wat, M.B. Comfort, Peri-implant bone loss: management of a patient, Int. J. Oral Maxillofac. Implants 16 (2) (2001) 273–277.
[9] F. Isidor, Influence of forces on peri-implant bone, Clin. Oral Implants Res. 17 (Suppl. 2) (2006) 8–18.
[10] L.F. Tabata, E.P. Rocha, V.A. Barão, W.G. Assunção, Platform switching: biomechanical evaluation using three-dimensional finite element analysis, Int. J. Oral Maxillofac. Implants 26 (3) (2011) 482–491.
[11] T. Shapurian, P.D. Damoulis, G.M. Reiser, T.J. Griffin, W.M. Rand, Quantitative evaluation of bone density using the hounsfield index, Int. J. Oral Maxillofac. Implants 21 (2) (2006) 290–297.
[12] N.A. Drage, R.M. Palmer, G. Blake, R. Wilson, F. Crane, I. Fogelman, A comparison of bone mineral density in the spine, hip and jaws of edentulous subjects, Clin. Oral Implants Res. 18 (4) (2007) 496–500.
[13] M. Yamazaki, T. Shirota, Y. Tokugawa, M. Motohashi, K. Ohno, K. Michi, et al., Bone reactions to titanium screw implants in ovariectomized animals, Oral Surg. Oral Med. Oral Pathol. Oral Radiol. Endod. 87 (4) (1999) 411–418.
[14] S. Ozawa, T. Ogawa, K. Iida, C. Sukotjo, H. Hasegawa, R.D. Nishimura, et al., Ovariectomy hinders the early stage of bone-implant integration: histomorphometric, biomechanical, and molecular analyses, Bone 30 (1) (2002) 137–143.
[15] S. Khosla, S. Amin, E. Orwoll, Osteoporosis in men, Endocr. Rev. 29 (4) (2008) 441–464.
[16] M.T. Drake, S. Khosla, Male osteoporosis, Endocrinol. Metab. Clin. N. Am. 41 (3) (2012) 629–641.
[17] A. Giusti, G. Bianchi, Treatment of primary osteoporosis in men, Clin. Interv. Aging 10 (2015) 105–115.
[18] R. Niimi, T. Kono, A. Nishihara, M. Hasegawa, A. Matsumine, T. Kono, et al., Analysis of daily teriparatide treatment for osteoporosis in men, Osteoporos. Int. 26 (4) (2015) 1303–1309.
[19] P. Farahmand, R. Spiegel, J.D. Ringe, Male osteoporosis, Z. Rheumatol. 75 (5) (2016) 459–465.
[20] J.S. Finkelstein, A. Hayes, J.L. Hunzelman, J.J. Wyland, H. Lee, R.M. Neer, The effects of parathyroid hormone, alendronate, or both in men with osteoporosis, N. Engl. J. Med. 349 (13) (2003) 1216–1226.
[21] D. Vanderschueren, L. Vandenput, S. Boonen, M.K. Lindberg, R. Bouillon, C. Ohlsson, Androgens and bone, Endocr. Rev. 25 (3) (2004) 389–425.
[22] G. Qian, L. Zhang, G. Wang, Z. Zhao, S. Peng, C. Shuai, 3D printed zn-doped mesoporous silica-incorporated poly-L-lactic acid scaffolds for bone repair, Int. J. Bioprint. 7 (2) (2021) 346.
[23] G. Qian, P. Fan, F. He, J. Ye, Novel strategy to accelerate bone regeneration of calcium phosphate cement by incorporating 3D plotted poly(lactic-co-glycolic acid) network and bioactive wollastonite, Adv. Healthc. Mater. 8 (9) (2019), e1801325.
[24] D. de Oliveira, Puttini I. de Oliveira, P.H. Silva Gomes-Ferreira, L.P. Palin, M.A. Matsumoto, R. Okamoto, Effect of intermittent teriparatide (PTH 1–34) on the alveolar healing process in orchiectomized rats, Clin. Oral Investig. 23 (5) (2019) 2313–2322.
[25] Puttini I. de Oliveira, P. Gomes-Ferreira, D. de Oliveira, J.S. Hassumi, P.Z. Gonçalves, R. Okamoto, Teriparatide improves alveolar bone modelling after tooth extraction in orchiectomized rats, Arch. Oral Biol. 102 (2019) 147–154.
[26] P.H.S. Gomes-Ferreira, P.N. Lisboa-Filho, A.C. da Silva, O. Bim-Júnior, F.R. de Souza Batista, A.C. Ervolino-Silva, et al., Sonochemical time standardization for bioactive materials used in periimplantar defects filling, Ultrason. Sonochem. 56 (2019) 437–446.
[27] A.A. Veis, N.N. Dabarakis, N.A. Parisis, A.T. Tsirlis, T.G. Karanikola, D.V. Printza, Bone regeneration around implants using spherical and granular forms of bioactive glass particles, Implant. Dent. 15 (4) (2006) 386–394.
[28] L.B. Arruda, M.O. Orlandi, P.N. Lisboa-Filho, Morphological modifications and surface amorphization in ZnO sonochemically treated nanoparticles, Ultrason. Sonochem. 20 (3) (2013) 799–804.
[29] A. Hoppe, N.S. Güldal, A.R. Boccaccini, A review of the biological response to ionic dissolution products from bioactive glasses and glass-ceramics, Biomaterials 32 (11) (2011) 2757–2774.

[30] A.M. El-Kady, M.M. Farag, Bioactive glass nanoparticles as a new delivery system for sustained 5-fluorouracil release: characterization and evaluation of drug release mechanism, J. Nanomater. 2015 (2015), 839207.
[31] X. Du, Z. Li, J. Xia, F. Zhang, Z. Wang, Facile sonochemistry-assisted assembly of the water-loving drug-loaded micro-organogel with thermo- and redox-sensitive behavior, Colloids Surf. A Physicochem. Eng. Asp. (2018) 561.
[32] A.R. Al-Shahat, M.A. Shaikh, R.A. Elmansy, K. Shehzad, Z.A. Kaimkhani, Prostatic assessment in rats after bilateral orchidectomy and calcitonin treatment, Endocr. Regul. 45 (1) (2011) 29–36.
[33] P.H.S. Gomes-Ferreira, D. de Oliveira, P.B. Frigério, F.R. de Souza Batista, K. Grandfield, R. Okamoto, Teriparatide improves microarchitectural characteristics of peri-implant bone in orchiectomized rats, Osteoporos. Int. 31 (9) (2020) 1807–1815.
[34] Z.S. Tao, W.S. Zhou, X.J. Wu, L. Wang, M. Yang, J.B. Xie, et al., Single-dose local administration of parathyroid hormone (1–34, PTH) with β-tricalcium phosphate/collagen (β-TCP/COL) enhances bone defect healing in ovariectomized rats, J. Bone Miner. Metab. 37 (1) (2019) 28–35.
[35] E.R. Luvizuto, S.S. Dias, T. Okamoto, R.C. Dornelles, R. Okamoto, Raloxifene therapy inhibits osteoclastogenesis during the alveolar healing process in rats, Arch. Oral Biol. 56 (10) (2011) 984–990.
[36] G. Ramalho-Ferreira, L.P. Faverani, F.B. Prado, I.R. Garcia Jr., R. Okamoto, Raloxifene enhances peri-implant bone healing in osteoporotic rats, Int. J. Oral Maxillofac. Surg. 44 (6) (2015) 798–805.
[37] C. Johansson, T. Albrektsson, Integration of screw implants in the rabbit: a 1-year follow-up of removal torque of titanium implants, Int. J. Oral Maxillofac. Implants 2 (2) (1987) 69–75.
[38] D.W. Dempster, J.E. Compston, M.K. Drezner, F.H. Glorieux, J.A. Kanis, H. Malluche, et al., Standardized nomenclature, symbols, and units for bone histomorphometry: a 2012 update of the report of the ASBMR histomorphometry nomenclature committee, J. Bone Miner. Res. 28 (1) (2013) 2–17.
[39] C. Micheletti, P.H.S. Gomes-Ferreira, T. Casagrande, P.N. Lisboa-Filho, R. Okamoto, K. Grandfield, From tissue retrieval to electron tomography: nanoscale characterization of the interface between bone and bioactive glass, J. R. Soc. Interface 18 (182) (2021) 20210181.
[40] J.M. Kaufman, B. Lapauw, S. Goemaere, Current and future treatments of osteoporosis in men, Best Pract. Res. Clin. Endocrinol. Metab. 28 (6) (2014) 871–884.
[41] F.A. Santos, M.T. Pochapski, M.C. Martins, E.G. Zenóbio, L.C. Spolidoro, E. Marcantonio Jr., Comparison of biomaterial implants in the dental socket: histological analysis in dogs, Clin. Implant. Dent. Relat. Res. 12 (1) (2010) 18–25.
[42] R.D.S. Pereira, J.D. Menezes, J.P. Bonardi, G.L. Griza, R. Okamoto, E. Hochuli-Vieira, Histomorphometric and immunohistochemical assessment of RUNX2 and VEGF of Biogran™ and autogenous bone graft in human maxillary sinus bone augmentation: a prospective and randomized study, Clin. Implant. Dent. Relat. Res. 19 (5) (2017) 867–875.
[43] T. Taghipour, G. Karimipour, M. Ghaedi, A. Asfaram, Mild synthesis of a Zn(II) metal organic polymer and its hybrid with activated carbon: application as antibacterial agent and in water treatment by using sonochemistry: optimization, kinetic and isotherm study, Ultrason. Sonochem. 41 (2018) 389–396.
[44] M. Sjöström, S. Lundgren, H. Nilson, L. Sennerby, Monitoring of implant stability in grafted bone using resonance frequency analysis. A clinical study from implant placement to 6 months of loading, Int. J. Oral Maxillofac. Surg. 34 (1) (2005) 45–51.
[45] J.R. Jones, Review of bioactive glass: from hench to hybrids, Acta Biomater. 9 (1) (2013) 4457–4486.
[46] K. Grandfield, A. Palmquist, F. Ericson, J. Malmström, L. Emanuelsson, C. Slotte, et al., Bone response to free-form fabricated hydroxyapatite and zirconia scaffolds: a transmission electron microscopy study in the human maxilla, Clin. Implant. Dent. Relat. Res. 14 (3) (2012) 461–469.
[47] D.M. Binkley, J. Deering, H. Yuan, A. Gourrier, K. Grandfield, Ellipsoidal mesoscale mineralization pattern in human cortical bone revealed in 3D by plasma focused ion beam serial sectioning, J. Struct. Biol. 212 (2) (2020), 107615.
[48] K. Grandfield, V. Vuong, H.P. Schwarcz, Ultrastructure of bone: hierarchical features from nanometer to micrometer scale revealed in focused ion beam sections in the TEM, Calcif. Tissue Int. 103 (6) (2018) 606–616.
[49] F.A. Shah, K. Ruscsák, A. Palmquist, Transformation of bone mineral morphology: from discrete marquise-shaped motifs to a continuous interwoven mesh, Bone Rep. 13 (2020), 100283.
[50] Q. Wang, T. Tang, D. Cooper, F. Eltit, P. Fratzl, P. Guy, et al., Globular structure of the hypermineralized tissue in human femoral neck, J. Struct. Biol. 212 (2) (2020), 107606.
[51] R.E. Jung, G.A. Hälg, D.S. Thoma, C.H. Hämmerle, A randomized, controlled clinical trial to evaluate a new membrane for guided bone regeneration around dental implants, Clin. Oral Implants Res. 20 (2) (2009) 162–168.
[52] A. Blumsohn, F. Marin, T. Nickelsen, K. Brixen, G. Sigurdsson, J. González de la Vera, et al., Early changes in biochemical markers of bone turnover and their relationship with bone mineral density changes after 24 months of treatment with teriparatide, Osteoporos. Int. 22 (6) (2011) 1935–1946.